\$ SUPER

Contents lists available at ScienceDirect

# Global and Planetary Change

journal homepage: www.elsevier.com/locate/gloplacha



# Relative sea-level change in South Florida during the past ~5000 years

Nicole S. Khan <sup>a,b,\*</sup>, Erica Ashe <sup>c</sup>, Ryan P. Moyer <sup>d</sup>, Andrew C. Kemp <sup>e</sup>, Simon E. Engelhart <sup>f</sup>, Matthew J. Brain <sup>f</sup>, Lauren T. Toth <sup>b</sup>, Amanda Chappel <sup>d,g</sup>, Margaret Christie <sup>h</sup>, Robert E. Kopp <sup>c,i</sup>, Benjamin P. Horton <sup>j,k</sup>

- a Department of Earth Sciences and the Swire Institute of Marine Science, The University of Hong Kong, Hong Kong
- <sup>b</sup> U.S. Geological Survey, St Petersburg Coastal and Marine Science Center, St Petersburg, FL, USA
- <sup>c</sup> Department of Earth and Planetary Sciences, Rutgers University, Piscataway, NJ, USA
- d Fish and Wildlife Research Institute, Florida Fish and Wildlife Conservation Commission, St Petersburg, FL, USA
- <sup>e</sup> Department of Earth and Climate Sciences, Tufts University, Medford, MA, USA
- <sup>f</sup> Department of Geography, Durham University, Durham, UK
- <sup>g</sup> Department of Environmental Engineering Science, University of Florida, Gainesville, FL, USA
- h Department of Environmental Studies, McDaniel College, Westminster, MD, USA
- <sup>i</sup> Rutgers Institute of Earth, Ocean, and Atmospheric Sciences, Rutgers University, Piscataway, NJ, USA
- <sup>j</sup> Earth Observatory of Singapore, Nanyang Technological University, Singapore
- <sup>k</sup> Asian School of the Environment, Nanyang Technological University, Singapore

#### ARTICLE INFO

Editor: Dr. Fabienne Marret-Davies

Keywords: Sea level Holocene Mangrove Proxy reconstruction Reproducibility

#### ABSTRACT

A paucity of detailed relative sea-level (RSL) reconstructions from low latitudes hinders efforts to understand the global, regional, and local processes that cause RSL change. We reconstruct RSL change during the past ~5 ka using cores of mangrove peat at two sites (Snipe Key and Swan Key) in the Florida Keys. Remote sensing and field surveys established the relationship between peat-forming mangroves and tidal elevation in South Florida. Core chronologies are developed from age-depth models applied to 72 radiocarbon dates (39 mangrove wood macrofossils and 33 fine-fraction bulk peat). RSL rose 3.7 m at Snipe Key and 5.0 m at Swan Key in the past 5 ka, with both sites recording the fastest century-scale rate of RSL rise since  $\sim$ 1900 CE ( $\sim$ 2.1 mm/a). We demonstrate that it is feasible to produce near-continuous reconstructions of RSL from mangrove peat in regions with a microtidal regime and accommodation space created by millennial-scale RSL rise. Decomposition of RSL trends from a network of reconstructions across South Florida using a spatio-temporal model suggests that Snipe Key was representative of regional RSL trends, but Swan Key was influenced by an additional local-scale process acting over at least the past five millennia. Geotechnical analysis of modern and buried mangrove peat indicates that sediment compaction is not the local-scale process responsible for the exaggerated RSL rise at Swan Key. The substantial difference in RSL between two nearby sites highlights the critical need for within-region replication of RSL reconstructions to avoid misattribution of sea-level trends, which could also have implications for geophysical modeling studies using RSL data for model tuning and validation.

## 1. Introduction

Relative sea level (RSL) is the net outcome of a variety of physical processes operating on characteristic spatial (local to global) and temporal (minutes to millennia) scales. Consequently, similarities and differences in RSL across space and through time are interpreted in terms of their underlying causes to better understand specific processes. Prior to systematic tide-gauge measurements (since  $\sim\!1900$  CE in the southeastern United States), patterns of RSL change have been reconstructed

using proxies preserved in geological archives, such as salt-marsh sediment (e.g., van de Plassche et al., 1998; Gehrels et al., 2008; Long et al., 2012; Walker et al., 2021), coral microatolls (Goodwin and Harvey, 2008; Woodroffe et al., 2012; Hallmann et al., 2018), bioconstructed reefs (Suguio and Martin, 1978; Angulo et al., 1999), and archeological features (Sivan et al., 2004; Dean et al., 2019). Reconstructions of late Holocene RSL change demonstrate that the high rate of rise since the mid-19th century was a global phenomenon and without precedent in at least the preceding ~3 ka (e.g., Kemp et al., 2018; Kopp et al., 2016).

<sup>\*</sup> Corresponding author at: Department of Earth Sciences and the Swire Institute of Marine Science, The University of Hong Kong, Hong Kong. *E-mail address:* nskhan@hku.hk (N.S. Khan).

Along the Atlantic coast of North America, salt-marsh records also identified earlier phases of regional- and (multi-) centennial-scale sealevel variability. Efforts to differentiate between possible causes for this earlier sea-level variability (e.g., land ice melt and/or redistribution of existing ocean mass by prevailing winds and ocean currents) are hindered by a paucity of near-continuous reconstructions south of Cape Hatteras in the Western Atlantic (Fig. 1) and from low latitudes more broadly. Recognizing the role of processes causing regional-scale RSL change is also important for anticipating future sea-level trends,

particularly in South Florida where densely-populated urban areas, aging flood-control facilities, flat topography, and porous limestone bedrock heighten socio-economic vulnerability to future RSL rise (e.g., Noss, 2011).

Along the Atlantic coast of North America, near-continuous reconstructions of late Holocene RSL are almost exclusively generated from sequences of sediment deposited in high salt-marsh environments (e.g., Gehrels et al., 2020; Kemp et al., 2018). In South Florida, salt marshes are replaced by mangroves and it is unclear if these

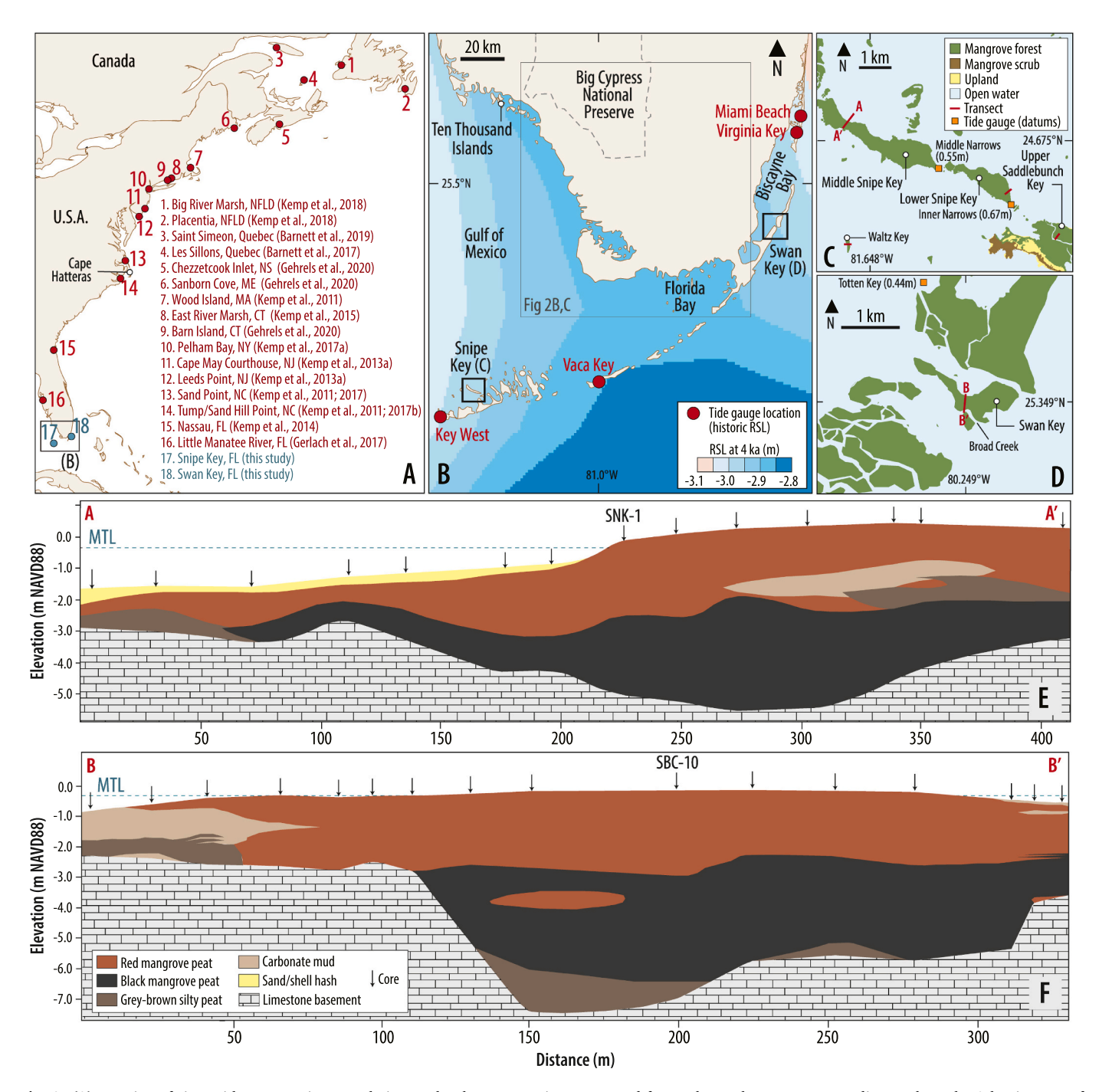


Fig. 1. (A) Location of sites with near-continuous relative sea-level reconstructions generated from salt-marsh or mangrove sediment along the Atlantic coast of North America. (B) Study sites and tide gauges with historic sea-level measurements in South Florida. Shading of ocean represents relative sea level predicted at 4 ka by a glacial-isostatic adjustment model (ICE-7G\_NA VM7; Roy and Peltier, 2017). (C, D) Locations of transects where the elevational range of peat-forming mangroves was measured. At Snipe Key and Swan Key cores collected along each transect were used to describe the underlying stratigraphy (panels E and F respectively). Select tide gauges deployed by NOAA to establish tidal datums are shown; presented values are for great diurnal tidal range (mean lower low water to mean higher high water). MTL: mean tide level. (Kemp et al., 2015, Kemp et al., 2013; Kemp et al., 2015; Barnett et al., 2017; Barnett et al., 2019).

environments can generate RSL reconstructions of comparable accuracy and precision (vertical and temporal) to those from salt marshes. Specifically, bioturbation (e.g., Ellison, 2008; McKee and Faulkner, 2000; Woodroffe et al., 2015b) and poor preservation of micro- and macrofossils (e.g., Berkeley et al., 2009; Debenay et al., 2004) present challenges to deriving robust chronologies and detailed RSL reconstructions from mangrove sediment. Given the resources required to produce a near-continuous RSL reconstruction, the sea-level research community has understandably prioritized producing new records to explore sea-level variability among regions, rather than replicating RSL records within regions. However, this sampling regime is ill-suited to robustly differentiate the influence of regional- and local-scale processes, with the risk that reconstructed RSL trends will be misattributed to specific processes.

To expand the latitudinal range and density of late Holocene RSL reconstructions along the Atlantic coast of North America and evaluate the within-region replicability of RSL reconstructions (Kemp et al., 2017b; Kemp et al., 2018), we develop new records from two sites (Snipe Key and Swan Key; Fig. 1) separated by ∼160 km in South Florida. These near-continuous reconstructions are generated from dated sequences of mangrove peat that accumulated during the past  $\sim$ 5 ka. We demonstrate that mangrove peat can be a source of detailed RSL reconstructions in regions experiencing long-term RSL rise with small tidal range, even if foraminifera (and/or other microfossil proxies) are poorly preserved or absent. We use a spatio-temporal empirical hierarchical model to decompose RSL trends from a network of reconstructions into regionaland local-scale signals. This analysis indicates that Snipe Key reflected regional-scale trends, but that Swan Key experienced additional RSL rise on millennial timescales from local-scale processes other than sediment compaction.

#### 2. Study area

The Florida Keys are a chain of small limestone islands that extend ~240 km from southern Miami to Key West, Florida (Fig. 1) and are underlain by the Key Largo Limestone and Miami Limestone formations (Sanford, 1909; Scott, 2001) that formed during the Last Interglacial period (Coniglio and Harrison, 1983). Low-energy, intertidal environments on the islands (keys) are commonly vegetated by peat-forming mangroves established when the rate of deglacial RSL rise slowed to <~5 mm/a at approximately 6-4 ka (Willard and Bernhardt, 2011; Dekker et al., 2015; Saintilan et al., 2020). The mangroves can be classified into fringe, basin, scrub, riverine, overwash, or hammock forests (Lugo and Snedaker, 1974) occupied by Rhizophora mangle (red), Avicennia germinans (black), and Laguncularia racemosa (white). In South Florida, monospecific stands of R. mangle occur at the lowest elevations fringing bays and tidal channels, and monospecific stands of R. mangle or mixed species stands of R. mangle, A. germinans, and L. racemosa occupy basins in the interior of mangrove islands (Scholl, 1964; Radabaugh et al., 2017).

Exploration of sites in the lower Florida Keys revealed Snipe Key to be underlain by a thick and continuous sequence of mangrove peat that was judged likely to produce a late Holocene RSL record. Snipe Key is a mangrove island containing fringe and basin monospecific and mixed stands of R. mangle, A. germinans, and L. racemosa (Fig. 1). A nearby (<3 km) tide gauge at Middle Narrows (NOAA station 8724427; Fig. 1C) measured great diurnal tidal range (mean lower low water, MLLW to mean higher high water, MHHW) to be 0.55 m. Swan Key was selected for analysis because previous work by Robbin (1984) showed the site to be underlain by a near-continuous sequence of mangrove peat that accumulated during the past  $\sim$ 5 ka. This mangrove island is occupied by monospecific and mixed fringe, scrub, and basin stands of R. mangle, A. germinans, and L. racemosa. A nearby (~2 km) tide gauge at Totten Key (NOAA station 8723467; Fig. 1D) measured great diurnal tidal range to be 0.44 m. In the Florida Keys, water heights display pronounced seasonality due to the steric effects of strong heating/cooling and salinity

changes in the Gulf of Mexico and seasonal winds (Liu and Weisberg, 2012). Lower water levels occur between January and July and elevated water levels occur from August to December. To provide a more complete characterization of contemporary mangrove environments and sediments, we conducted surveys at three additional sites (Fig. 1C; Fig. 2A). Lower Snipe Key and Waltz Key have similar vegetation composition and geomorphology to Swan Key and Snipe Key, while Upper Saddlebunch Key is occupied by scrub mangroves (suffering stunted growth due to nutrient limitation or salinity stress; e.g., Lugo and Snedaker, 1974).

#### 3. Methods and results

#### 3.1. Indicative meaning of mangroves in South Florida

The vertical distribution of mangroves is controlled by the frequency and duration of tidal inundation, which is principally a function of elevation (Ellison, 1993; Spalding et al., 2010; Woodroffe et al., 2016). The indicative meaning quantifies the relationship between a sea-level proxy and tidal elevation from modern observations (e.g., van de Plassche et al., 1998). To reconstruct RSL using mangroves as a proxy requires that they be assigned an indicative meaning established from measurements of modern mangroves. Peat-forming mangroves are putatively confined to the upper half of the intertidal zone from mean tide level (MTL) to highest astronomical tide (HAT) (Thom, 1967; Davis and Fitzgerald, 2003; Woodroffe et al., 2016; Khan et al., 2017; Chua et al., 2021), but surveys to quantify the indicative meaning of mangroves are rare (Leong et al., 2018) and restricted to a handful of sites assumed to be representative of regional patterns. Furthermore, the distribution of mangroves within their indicative range is poorly characterized, despite an implicit assumption in most subsequent statistical analyses of a normal distribution (e.g., Khan et al., 2017). We quantified the indicative meaning of mangroves in South Florida using two complementary approaches: (1) we surveyed the distribution of mangroves along transects at five sites in the lower and upper Florida Keys (Figs. 1, 2); and (2) we used remote sensing products to quantify the distribution of mangroves across a wide geographic area in South Florida (Fig. 2).

At the five sites in the Florida Keys (Snipe Key, Lower Snipe Key, Swan Key, Waltz Key, and Upper Saddlebunch Key), we established a transect through the intertidal zone. At evenly-spaced intervals of distance (in basin environments with flat topography) or elevation (in fringe environments with an elevation gradient) along each transect, we recorded qualitative surface sediment lithology. The elevation of each sampling location relative to a temporary benchmark was surveyed using an automatic level. At Waltz Key the tidal elevation of the temporary benchmark was measured directly by including tidal benchmarks in the survey. At the four other sites, we measured the elevation of temporary benchmarks relative to the North American Vertical Datum of 1988 (NAVD88) using a Leica GS15 global navigation system (Snipe Key) or an Ashtech differential global positioning system (Lower Snipe Key, Swan Key, Upper Saddlebunch Key). Elevations were converted from NAVD88 to tidal datums using VDatum (Yang et al., 2012). To account for differences in tidal range among sites, elevations were converted to standardized water level index (SWLI) units (Horton and Edwards, 2005), where a value of 0 corresponds to local MTL and a value of 100 corresponds to local MHHW. Along these transects the elevation of peat-forming mangroves is well described by a normal distribution with a mean and standard deviation of 120  $\pm$  59 SWLI units (Fig. 2; Table S1). The highest occurrence of peat-forming mangroves (termed HOP) occurred  $\sim 0.1-0.3$  m above highest astronomical tide (HAT), likely due to high seasonal variability in water levels superimposed on a microtidal regime, which causes seasonal water levels to regularly exceed HAT (a predicted astronomical tide; Kemp et al., 2022).

In our remote sensing analysis of regional-scale mangrove distribution in the Florida Everglades, we combined a map of vegetation cover derived from aerial photographs (Madden et al., 1999; Welch et al.,

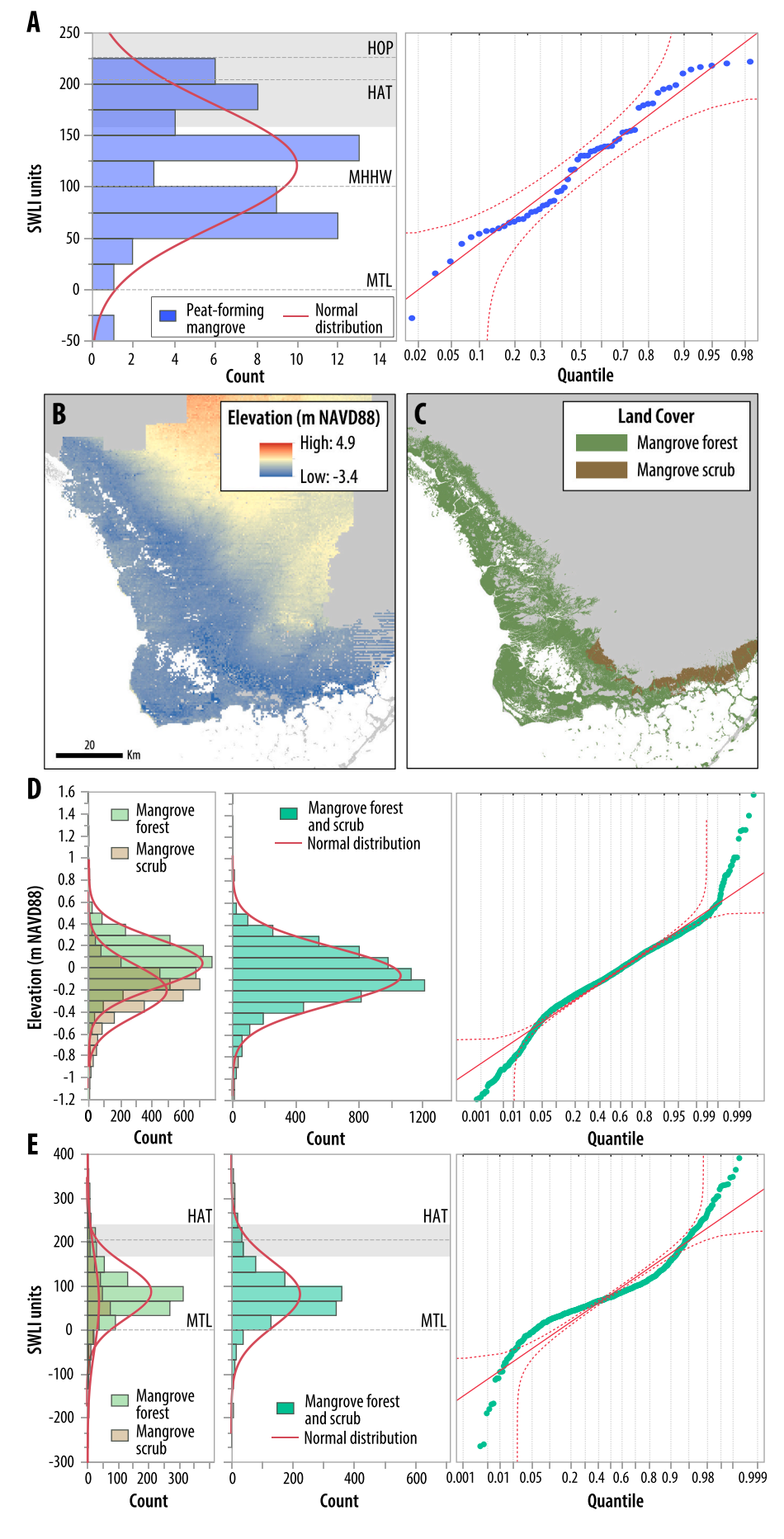


Fig. 2. Modern elevation distribution of mangroves from South Florida. (A) Elevation of peat-forming mangroves measured along surface transects at five sites in the Florida Keys. Location of surface transects is shown in Fig. 1C, D. Elevation is expressed as a standardized water level index (SWLI). (B-C) Geospatial datasets (South Florida Information Access digital elevation model from Desmond (2003) [B] and Center for Remote Sensing and Mapping Science land cover vegetation map from Madden et al. (1999) and Welch et al. (1999) [C]) were used to derive the mangrove elevation dataset shown in D (expressed relative to the North Atlantic Vertical Datum [NAVD88]) and E (expressed in SWLI units). VDatum was used to convert orthometric heights to local tidal levels; many of the orthometric point coordinates (D) were outside of the VDatum conversion grid, resulting in a much smaller elevation dataset (E). (D, E) Elevation distribution in NAVD88 (D) and SWLI units (E) and Q-Q plot of forest and scrub mangroves estimated from the elevation datasets from B and C. Normal distributions were fitted to elevation distributions shown in A, D, and E, and the fit was assessed by the Q-Q plot (blue and green circles show the empirical cumulative probability of the elevation dataset, red lines show the normal theoretical quantiles and Lilliefors confidence bounds [Conover, 1980)]) and measures presented in Table S1. (See Section 3.1 for further details). MTL: mean tide level; HAT: Highest astronomical tide. Note that mean (dotted line) and standard deviation (gray shading) of HAT from nearby tide gauges (Table S4) is shown in A and E. (For interpretation of the references to color in this figure legend, the reader is referred to the web version of this article.)

1999) with the South Florida Information Access digital elevation model (400 m  $\times$  400 m grid with vertical accuracy of  $\pm 15$  cm; Desmond, 2003). For each polygon of mangrove forest or mangrove scrub, an elevation point was extracted from the corresponding location in the model using the intersection tool in ArcGIS. We used VDatum to convert each elevation from NAVD88 to tidal datums and calculate a SWLI. Because some locations are outside the bounds of VDatum, the conversion from NAVD88 caused a reduction in the number of observations (from 6805 to 1255; Fig. 2; Table S1). We analyzed the elevations of mangrove forest and scrub separately and then together. The distribution of the separate groups is reasonably well approximated by a normal distribution of 86  $\pm$  61 SWLI (mean  $\pm$  standard deviation) for mangrove forest compared to 61  $\pm$  105 SWLI for scrub mangroves (Fig. 2; Table S1). When combined, the distribution remains approximately normal (81  $\pm$  74 SWLI). These distributions are not directly comparable to the field survey of peat-forming mangroves because the remote sensing analyses included all areas of mangrove cover regardless of their underlying substrate, which can likely grow at lower (non-peat-forming) elevations below MTL (e.g., Khan et al., 2019).

From the survey and remote sensing analyses of mangrove distribution by tidal elevation, we adopted a conservative indicative meaning of MTL to HOP (95% confidence) for undifferentiated mangrove peat recovered in cores. This range is likely large enough to encompass all species of mangrove and their geomorphic settings in South Florida and can be reasonably approximated by a normal distribution in statistical analyses. For studies that do not differentiate between peat-forming mangroves and other types of mangrove sediments (e.g., muds and sands), an alternative indicative meaning may be more appropriate.

#### 3.2. Mangrove stratigraphy

Similar stratigraphic sequences were identified at Snipe Key and Swan Key using hand-driven cores collected along transects (Fig. 1E, F). Core-top elevations were measured using the same approach employed for surface sediment (Section 3.1). Overlying the limestone basement, two principal lithologic units were identified, a black mangrove peat at the base of the sequence and a red mangrove peat at the top of the sequence (descriptions refer to sediment color rather than the dominant peat-forming mangrove species). The black mangrove peat consisted of decomposed organic material with identifiable *R. mangle* mangrove remains (leaf and wood fragments and roots). The red mangrove peat was primarily composed of fine *R. mangle* roots.

Cores SNK1 from Snipe Key (24.679 °N, -81.653 °E) and SBC10 from Swan Key (25.349 °N, -80.251 °E) were selected for detailed analysis because they contained thick sequences of continuous mangrove peat that were deemed representative of the stratigraphy underlying each site (Fig. 1). In SNK1, black mangrove peat at depths of 4.9 to 2.4 m was conformably overlain by red mangrove peat (gradational contact) from 2.4 m to the core top (0.31 m MTL). In SBC10, black mangrove peat extending from 7.5 to 2.7 m was also conformably overlain by red mangrove peat (gradational contact) from 2.7 m to the top of the core (0.29 m MTL). The cores were collected in overlapping 0.5-m intervals using an Eijkelkamp peat sampler to prevent compaction and contamination during sampling. To minimize moisture loss and microbial activity, cores were placed in split PVC pipe, wrapped in plastic, and refrigerated prior to analysis. One replicate of each core was sampled for foraminiferal analysis within ~2 h of core collection by placing 1-cm thick samples into vials of buffered ethanol. Analysis of these samples followed standard methods (Horton and Edwards, 2006) and showed foraminifera to be present in the units of red and black mangrove peat in both cores, but in concentrations too low to generate statistically-robust counts (Kemp et al., 2020) in a reasonable time frame (Table S2).

#### 3.3. Sediment compaction

Mangrove sediments may compact, resulting in post depositional lowering (PDL) of samples used to reconstruct RSL (Bloom, 1964; Kaye and Barghoorn, 1964; Toscano et al., 2018). To estimate the contribution of compaction to reconstructed RSL, we used a three-stage geotechnical modeling approach developed for salt-marsh sediments (Brain, 2015). In step one, the compression behaviour of modern (surface) mangrove sediments was measured (Fig. 3A). We collected 16 modern samples (15-cm depth and diameter) from the range of contemporary eco-sedimentary zones encountered at Middle Snipe Key (n = 5), Lower Snipe Key (n = 6), and Swan Key (n = 5; Fig. 1; Table 1). For each sample, we measured (i) organic content by loss-on-ignition (LOI; three determinations per sample; e.g., Plater et al., 2015); (ii) particle density  $(G_s)$  using gas pycnometry; (iii) voids ratio  $(e_1)$  (one determination per sample; Head, 1988); and (iv) compression behaviour using automated oedometer testing (Head and Epps, 2011; Rees, 2014). LOI in 15 modern samples from peat-forming mangroves ranged from 57.5 to 75.8% (mean of 67.7%  $\pm$  4.4%, one standard deviation). One open-bay, sub-tidal sample composed of carbonate mud from Lower Snipe Key had a LOI of 24.4%.

In step two, we measured LOI and dry density in every other 1-cm thick sample in SNK1 and SBC10 (Fig. 3B, C) using the methods noted above. SNK1 had relatively uniform dry density (0.13  $\pm$  0.02 g/cm³), but LOI in the black mangrove peat (71.4  $\pm$  3.4%) was greater than in the red mangrove peat (62.4  $\pm$  7.1%), with a full range of 39.5–79.8%. Dry density (0.14  $\pm$  0.03 g/cm³) and LOI (63.1  $\pm$  3.4%) were relatively uniform within and between the units of black and red mangrove peat in SBC10. The observed LOI values in the cores overlap with those measured in our modern mangrove samples. As such, we deemed the properties measured on modern samples to be geotechnical analogues for core material.

In step three, compression properties were assigned to layers throughout each core based on their observed correlation with LOI in the modern dataset. We used the semi-empirical equation of Hobbs (1986) to predict downcore  $G_s$  from measured LOI in each layer during each model run; the regression model error was sampled from a uniform error distribution defined by the range of observed residuals. To assign values of  $C_r$  and  $C_c$  to layers in each core for each model run, we sampled from a uniform probability distribution defined by the range of values observed in our modern training set. We observed a statistically-significant relationship between LOI and  $e_1$  ( $r_{adj}^2 = 0.45$ ; p = 0.004). However, the form of this relationship ( $e_1 = 0.48*LOI - 20.51$ ) predicts physically improbable states for LOI values lower than ~40%. Given the poor constraint on the relationship provided by our modern mangrove samples, we assigned values of  $e_1$  by sampling from a uniform probability distribution defined by the range of values observed in our modern training set.

Estimates of effective stress and PDL are shown in Fig. 3B, C. Peak PDL was 2.6  $\pm$  0.1 cm in SNK1 (at 2.40 m depth) and 3.5  $\pm$  0.1 cm in SBC10 (at 3.38 m depth). Measured bulk density is within the one standard deviation range of values predicted by the model, supporting our approach.

### 3.4. Core chronologies

Sediment accumulation in SNK1 and SBC10 was determined by radiocarbon dating and recognition of pollution and land-use changes of known age in downcore profiles of elemental abundance and pollen assemblages (Tables 2–4). Where possible, plant macrofossils of mangrove wood (trunk or branches), terminal stems, and prop root bark were separated from the peat matrix for radiocarbon dating (Fig. S1). Plant macrofossils were identified with reference to published guides (e. g., Tomlinson, 2016) and fresh and subfossil (i.e., plant litter accumulating on the sediment surface at different states of decay) specimens collected at the field sites. We distinguished aboveground components of

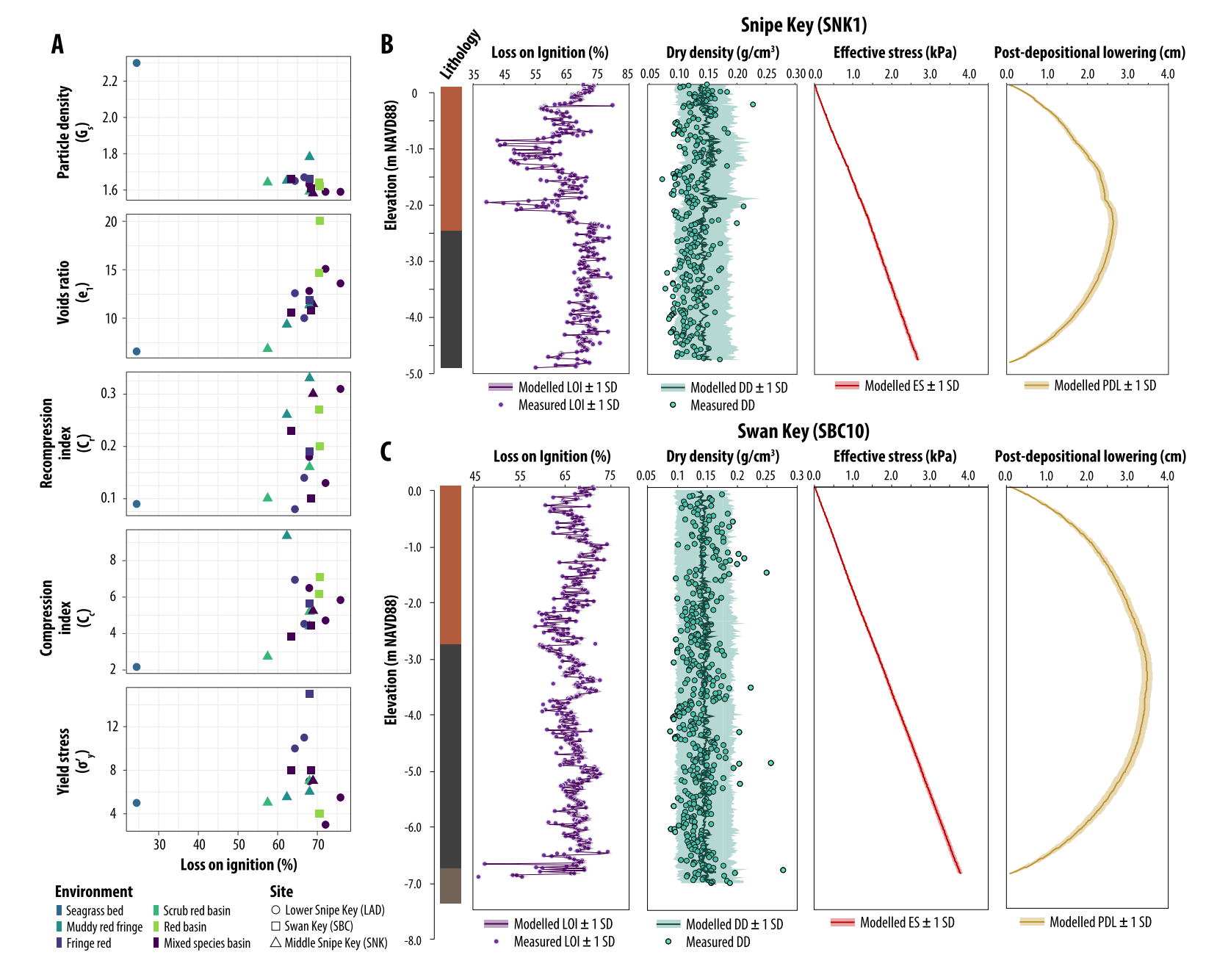


**Fig. 3.** (A) Observed relationships between geotechnical and physical properties of modern mangrove sediments collected at three sites (symbol shape) in the Florida Keys and across a range of ecological zones (symbol color). Due to the narrow range of measured loss-on-ignition (LOI) relative to compression behaviour, we did not observe statistically-significant relationships between LOI and particle density ( $G_s$ ;  $r_{adj}^2 = 0.03$ ; p = 0.251), recompression index ( $C_t$ ;  $r_{adj}^2 = 0.08$ ; p = 0.165), or compression index ( $C_c$ ;  $r_{adj}^2 = 0.001$ ; p = 0.560). (B, C) Estimation of post-depositional lowering (PDL) due to physical compression of core sediments. Comparisons of measured and model-predicted (mean and 95% credible interval) loss on ignition (purple) and dry bulk density (green) and modeled effective stress profiles and PDL estimates are shown for sediment samples from cores SNK1 (B) and SBC10 (C). (For interpretation of the references to color in this figure legend, the reader is referred to the web version of this article.)

**Table 1**Physical and geotechnical properties of modern mangrove sediments collected from Lower Snipe Key (LAD), Swan Key (SBC) and Middle Snipe Key (SNK). The recompression index,  $C_r$ , describes the compressibility of the sample in its pre-yield, reduced compressibility condition. The compression index,  $C_c$ , describes the compressibility of the sample in its post-yield, increased-compressibility condition. The yield stress,  $\sigma'_y$ , defines the transition from reduced-to increased-compressibility states.

Sample ID	Mangrove eco- sedimentary zone	Loss on ignition, LOI (%)	Particle density, $G_s$	Voids ratio at 1 kPa, $e_1$	Recompression index, $C_{\rm r}$	Compression index, $C_c$	Yield stress, $\sigma'_y$ (kPa)
LAD17/AC01	Mixed-species basin	67.97	1.63	12.84	0.18	6.50	7.0
LAD17/AC02	Mixed-species basin	72.07	1.59	15.12	0.13	4.72	3.0
LAD17/AC03	Mixed-species basin	75.84	1.59	13.62	0.31	5.84	5.5
LAD17/AC04	Fringe red	66.70	1.67	10.04	0.14	4.53	11.0
LAD17/AC05	Fringe red	64.35	1.65	12.61	0.08	6.95	10.0
LAD17/AC06	Mud flat/open bay/	24.44	2.30	6.60	0.09	2.17	5.0
	seagrass bed						
SBC17/AC01	Muddy red fringe	62.32	1.65	9.34	0.26	9.34	5.5
SBC17/AC02	Scrub red basin	68.04	1.59	11.41	0.16	5.18	7.0
SBC17/AC03	Scrub red basin	57.47	1.64	6.83	0.10	2.72	5.0
SBC17/AC04	Mixed-species basin	68.92	1.58	11.46	0.30	5.23	7.0
SBC17/AC05	Muddy red fringe	68.05	1.78	11.32	0.33	4.38	6.0
SNK17/AC01	Mixed-species basin	68.36	1.61	10.87	0.10	4.46	8.0
SNK17/AC02	Mixed-species basin	63.39	1.66	10.64	0.23	3.83	8.0
SNK17/AC03	Red basin	70.61	1.62	20.09	0.20	7.09	4.0
SNK17/AC04	Red basin	70.40	1.64	14.69	0.27	6.16	4.0
SNK17/AC05	Fringe red	68.09	1.66	11.88	0.19	5.64	15.0

mangrove wood from roots that formed belowground on the basis of the color, morphology, and rigidity of the plant material. The epidermis of coarse mangrove roots can be dark red or brown in color, with the interior portion darker in color than the exterior. These roots are also thin and flexible, and often lateral insertion points where smaller roots connected to larger ones can be observed. In contrast, aboveground wood components are much more rigid and dark brown to black in color (except for prop root bark that is a lighter shade of brown). With large enough macrofossils, prop root bark is identifiable by the presence of lenticels (small openings that provide gas exchange and an additional source of oxygen for the submersed roots), and terminal twigs can be identified by leaf scars (mark left by a leaf after it falls off the twig). These macrofossils likely formed within the paleomangrove stand (undergoing minimal transport) near-contemporaneously with the mangrove sediment surface. Macrofossils were cleaned under a binocular microscope to remove adhering older sediments and/or younger ingrown rootlets (Kemp et al., 2013b). Where mangrove macrofossils were absent, the fine-fraction of bulk peat was separated for dating following Woodroffe et al. (2015b). Briefly, 1-cm thick horizons of bulk peat were passed through a 63-µm sieve, and the <63-µm fraction was collected onto a previously baked GF/F (0.7 µm) fiberglass filter under vacuum. Samples were oven dried at 55 °C and sent to the National Ocean Science Accelerator Mass Spectrometer (NOSAMS) laboratory for radiocarbon dating. At NOSAMS, mangrove macrofossils were acid-base-acid pretreated and fine-grained bulk samples were acid pretreated prior to conversion to graphite. Acid washing of bulk sediment served to remove carbonates and fulvic acids. Carbonates (if present) are likely to be systematically older than the mangrove surface on which they were deposited, and in carbonate-rich environments, such as the Florida Keys, contamination of bulk sediment ages by allochthonous carbonate could bias radiocarbon ages. Fulvic (and humic) acids are considered to be active components of peat that may be mobile in the sediment column (and surrounding landscapes) and can potentially bias bulk sediment ages older or younger (Runge et al., 1973; Wild et al., 2013). No base washing was performed on the bulk sediment samples because its humified nature would result in considerable loss of mass (e. g., Shore et al., 1995). This decision was made in consultation with NOSAMS staff and implicitly assumes that the mass retained by not base washing is not systematically different in age to other fractions of carbon in the sediment.  $\delta^{13}C$  was measured on an aliquot of gas from each combusted sample (Table 3 and 4).

To measure downcore elemental abundance, samples from the upper 35 cm (2-cm intervals in the upper 10 cm and 1-cm intervals below) of

SNK1 and SBC10 were freeze dried, ground to a fine, homogenized powder and sent to the Meadowlands Environmental Research Institute laboratory for commercial analysis of elemental abundance by inductively coupled plasma mass spectrometry (ICP-MS). Unprocessed sediment samples (1 cm<sup>3</sup> at 4 cm intervals in the top 35 cm) were sent to LacCore at the University of Minnesota, where pollen slides were prepared according to the methods of Faegri and Iversen (1989). We counted 100 pollen grains and spores at 500× magnification; the low count was due to sparsity of pollen grains present in the samples. Assigning ages to downcore trends in elemental abundance and pollen requires recognizing the environmental impact of known historical events and/or trends (Table 2). Each age marker was assigned an age and depth uncertainty to account for the challenge of identifying a specific date in historical records, the possible lag between emission and deposition, and the possibility that horizons could be associated with multiple, adjacent depths in the core.

An age-depth model was developed for each core using Bchron (Fig. 4; Haslett and Parnell, 2008; Parnell et al., 2011) where input was radiocarbon dates and discrete age-depth estimates from marker horizons (assumed to have a normal probability distribution for age). All radiocarbon dates were calibrated by Bchron using the IntCal20 calibration curve (Reimer et al., 2020). Throughout the text, median and 95% credible interval age estimates derived from Bchron are reported.

The chronology for SNK1 was developed from 47 radiocarbon dates (Table 3; Khan et al., 2022) and two pollution horizons (Table 2). No pollen horizons representing land-use change or the introduction of exotic species were recognized in this core, likely because of its distance from population centers and agricultural activities, coupled with prevailing westerly winds that are unlikely to deliver pollen from South Florida (Christie et al., 2021). However, it is possible that low pollen counts may have contributed to the lack of signal. The core represents the past  $\sim\!5.9~\mathrm{ka}$  and the average age uncertainty for a 1-cm thick sample is  $\pm77~\mathrm{years}$ .

The chronology of SBC10 was derived from 43 radiocarbon dates (Table 4; Khan et al., 2022) and four pollen/pollution horizons. The core spans the past  $\sim\!6.3$  ka and the average age uncertainty for a 1-cm thick sample is  $\pm85$  years. Several radiocarbon dates (11 in SNK1 and eight in SBC10) were identified as outliers by Bchron in the lowermost section of both cores. Because the chronology obtained from these sections of core may be unreliable, we truncated both age models at the depth of the highest outliers at  $\sim\!5$  ka.

Table 2 Chronohorizons identified in cores SNK1 (Snipe Key) and SBC10 (Swan Key).

Age marker	Description	Age (CE)	SNK1	SBC10
Barium onset	Elevated Ba concentration due to the coincidence of an increase in oil-drilling (Swarzenski et al., 2006a; Carriquiry and Horta-Puga, 2010; Weerabaddana et al., 2021), changes in run- off or groundwater discharge (Swart et al., 1999; Swarzenski et al., 2006b), and increased	1970 ± 10	Increase in Ba from 4.0 to 22.2 mg/ kg at $5 \pm 4$ cm	Increase in Ba from 3.1 to 12.2 mg/kg at $7 \pm 4$ cm
Arsenic onset	phosphate mining (Froelich et al., 1985) Usage of arsenic-bearing herbicides applied to citrus fruit groves on industrial scales and local use on lawns and golf courses (Wojeck et al., 1982; Whitmore et al., 2008; Gerlach et al., 2017) Regional expansion of forestry and land	1955 ± 5	Increase in As from 12.1 to 23.2 mg/ kg at 9 $\pm$ 4 cm	Increase in As from 5.2 to 24.2 mg/kg at $9 \pm 9$ cm
<i>Pinus</i> decline	clearance resulting in the decline of <i>Pinus</i> in north-central (Johannes, 1976; Hoffman and Collopy, 1988; Kemp et al., 2014; Volk et al., 2017) and southern Florida (McAllister, 1938; Huck, 1995; Lauredo, 2018;	1935 ± 10	-	Decrease in <i>Pinus</i> pollen from >26 to 8% at $13.5 \pm 4$ cm
Casuarina arrival	Christie et al., 2021) The appearance of Casuarina pollen coincident with the known arrival of the non-native species brought to Florida to provide windbreak (Alexander and Crook, 1974; Morton, 1980; Wingard et al., 2007; Marshall et al., 2020)	1910 ± 15	-	Increase in Casuarina pollen from 0 to $>2\%$ at $25.5 \pm 5$ cm

## 3.5. Reconstruction of relative sea level

Relative sea level (RSL) was reconstructed using the equation:

$$RSL_{i} = Altitude_{i} - PME_{i}$$
 (1)

where the altitude of each sample i was measured directly as the depth below the core top of known tidal elevation and PME is paleo-mangrove elevation, which must be estimated using a sea-level proxy and expressed relative to the same tidal datums as altitude. In near-continuous, late Holocene RSL reconstructions, the most widely used proxy is salt-marsh foraminifera, and paleo marsh elevation is estimated for a subset of depths within the core at which foraminifera are counted. However, foraminifera were too sparse (but present throughout the units of red and black mangrove peat) in SNK1 and SBC10 (Table S2) to be employed as sea-level proxies (Kemp et al., 2020), which is common

for mangrove sediment (e.g., Berkeley et al., 2009; Woodroffe et al., 2015a). Therefore, we reconstructed PME by using sediment lithology to identify the likely environment of deposition. Samples identified as mangrove peat (recognized by the presence of mangrove terminal twigs, prop root bark, and roots) accumulated between local MTL and HOP (0.47  $\pm$  0.46 m MTL at Snipe Key and 0.38  $\pm$  0.37 m MTL at Swan Key). A RSL reconstruction was generated for each alternating 1-cm thick sample in the core, where sample age (with uncertainty) is from the age-depth model (Section 3.4).

During the past  $\sim$ 5 ka, Snipe and Swan Keys exhibited substantially different magnitudes of RSL rise. RSL rose at Snipe Key by 3.7 m (average of  $\sim$ 0.75 mm/a), compared to 5.0 m at Swan Key (average of  $\sim$ 1.0 mm/a; Fig. 5). At both sites the rate of RSL rise since  $\sim$ 1900 CE (2.0–2.1 mm/a) was the fastest during the past  $\sim$ 5 ka. Prior to the 20th century, the reconstructions indicate that there were multi-centennial phases of faster and slower RSL rise than the multi-millennial average. At both sites, the slowest rates of RSL rise occurred during the last millennium between  $\sim$ 1500 and 1800 CE ( $\sim$ 0.2 mm/a at Snipe Key and  $\sim$ 0.5 mm/a at Swan Key), between 2.1 and 1.9 ka ( $\sim$ 0.1 mm/a at Snipe Key and  $\sim$ 0.5 mm/a at Swan Key), and between 3.5 and 3.2 ka ( $\sim$ 0.2 mm/a at Snipe Key and  $\sim$ 0.5 mm/a at Swan Key) estimated by the spatio-temporal empirical hierarchical model (see Section 3.6 for more details).

We also compiled historic tide-gauge records (Fig. 6) and sea-level index points (Fig. 7) from the last 7 ka from South Florida (Love et al., 2016; Khan et al., 2017). We recalibrated the ages using the Intcal20 and Marine20 datasets (Heaton et al., 2020; Reimer et al., 2020) and  $\Delta R$ values from Toth et al. (2017a, 2017b) where appropriate. We also cross-checked and updated the index points with Acropora palmata coral data from Stathakopoulos et al. (2020), only using data that met the most stringent screening criteria (i.e., rank 0 in their taphonomicranking protocol) that assessed whether samples were in-situ on the reef when they were collected. There are typically a small number of coarse resolution (meter- and multi-century scale uncertainties) index points for any site in these databases. In South Florida, there are 55 index points from 28 sites, notably including 10 index points at Swan Key from the study of Robbin (1984) (Fig. 7c). Robbin (1984) sampled a vertical wall of mangrove peat on the channel branching northeast from Broad Creek on the south side of Swan Key (likely at B' on our coring transect) using horizontal push cores accessed via scuba diving from the channel cut to avoid compaction during coring. The interpretation of these data follows Love et al. (2016) and Khan et al. (2017), where an indicative meaning of MTL to HAT was adopted and combined with a number of conservative estimates of uncertainty associated with determining the depth and absolute elevation of the dated peat samples.

## 3.6. Spatio-temporal modeling

We employed a spatio-temporal empirical hierarchical model (STEHM; Ashe et al., 2019; Kopp et al., 2016) to examine the evolution of late Holocene RSL change in South Florida and explore possible driving mechanisms. Inputs for this model included: (1) the new proxy records from Swan and Snipe Keys; (2) tide-gauge records from South Florida (Fort Meyers, Naples, Key West, Key Colony Beach, Vaca Key, Virginia Key, Miami Beach, Lake Worth Pier; Fig. 1) longer than 11 years and within 1 degree (~110 km) of proxy data sites, which show consistent trends and variability in RSL over their period of operation (Fig. 6). Annual tide-gauge data were smoothed by fitting a temporal Gaussian Process model to each record and then transforming the fitted model to decadal averages, which more accurately reflect the recording capabilities of proxy records (Kopp et al., 2016); and (3) sea-level index points spanning the last 7 ka from South Florida (Love et al., 2016; Khan et al., 2017; Stathakopoulos et al., 2020).

The STEHM has three levels: (1) a data level, which models the way different proxies record RSL with vertical and temporal noise; (2) a process level, which distinguishes among RSL changes that are common

**Table 3** Radiocarbon ages from Core SNK1.

Sample ID	Depth (cm)	<sup>14</sup> C age (years)	Dated material	$\delta^{13}$ C (‰)	Outlier probability (%)	$2\sigma$ -calibrated age range (cal a BP)
OS-136048	20.5	$410\pm15$	<63 μm bulk peat	-21.7	0.01	462–505
OS-129399	27.5	$665\pm20$	<63 μm bulk peat	-22.8	0.00	562–668
OS-136049	37.5	$645\pm15$	<63 μm bulk peat	-20.1	0.02	560–655
OS-126725	49.5	$1140\pm15$	<63 μm bulk peat	-21.3	0.00	974–1173
OS-130926	65.5	$1330\pm15$	<63 μm bulk peat	-25.7	0.01	1178–1295
OS-129582	83.5	$1370\pm30$	Mangrove wood	-26.4	0.01	1179–1345
OS-130694	91.5	$1570\pm20$	Mangrove wood	-26.0	0.01	1395–1517
OS-130787	110.5	$1660\pm30$	Mangrove wood	-25.4	0.01	1416–1690
OS-136050	119.5	$1700\pm15$	<63 μm bulk peat	-24.7	0.01	1541–1689
OS-126753*	124.5	$3740\pm20$	<63 μm bulk peat	-30.2	1	_
OS-136051	130.5	$2120\pm15$	<63 μm bulk peat	-24.1	0.01	2003-2283
OS-130927	134.5	$2060\pm20$	<63 μm bulk peat	-24.6	0.03	1943-2100
OS-130928	152.5	$2540\pm20$	<63 μm bulk peat		0.03	2516–2740
OS-129581	162.5	$2520\pm20$	Mangrove wood	-25.2	0.01	2497–2726
OS-130974	171.5	$2540\pm20$	<63 µm bulk peat	-25.3	0.01	2516-2740
OS-130638	185.5	$2770\pm20$	Mangrove wood	-26.3	0.01	2785-2931
OS-126726*	197.5	$2910\pm20$	Mangrove wood	-27.0	1	_
OS-126795	197.5	$3180\pm20$	<63 µm bulk peat	-26.5	0.01	2964-3149
OS-130670	215.5	$2940\pm20$	Mangrove wood	-25.5	0.01	3004–3164
OS-138072*	220.5	$1640\pm20$	Mangrove wood	-25.8	1	_
OS-136221	227.5	$3100\pm20$	<63 µm bulk peat	-25.6	0.02	3245–3375
OS-129580	231.5	$3500\pm25$	<63 µm bulk peat	-26.7	0.01	3693-3841
OS-130695	245.5	$3620\pm20$	Mangrove wood	-25.7	0.01	3848–3982
OS-130975	263.5	$3720\pm25$	<63 µm bulk peat	-26.1	0.01	3982–4148
OS-126727	275.5	$3810\pm20$	<63 µm bulk peat	-26.6	0.01	4096-4288
OS-130976	286.5	$3910\pm20$	<63 µm bulk peat	-26.4	0.01	4254-4416
OS-129579	298.5	$3940\pm25$	Mangrove wood	-26.3	0.01	4260-4513
OS-130977	313.5	$4150\pm20$	<63 µm bulk peat	-26.5	0.01	4580-4822
OS-130669	313.5	$4180 \pm 20$	Mangrove wood	-26.6	0.01	4621–4831
OS-130978	330.5	$4320 \pm 20$	<63 µm bulk peat	-26.2	0.01	4840–4930
OS-126796	342.5	$4350\pm25$	Mangrove wood	-27.2	0.01	4850–4972
OS-130979	358.5	$4350 \pm 20$	<63 μm bulk peat	-26.3	0.01	4855–4964
OS-130696*	370.5	$4590 \pm 20$	Mangrove wood	-27.7	0.95	_
OS-129578	385.5	$4450 \pm 30$	Mangrove wood	-27.3	0.01	4886–5283
OS-138073	390.5	$4440 \pm 25$	Mangrove wood	-25.9	0.01	4882–5277
OS-130980*	399.5	$4710 \pm 20$	<63 μm bulk peat	-26.6	1	-
OS-136222	405.5	$4470 \pm 25$	<63 μm bulk peat	-25.9	0.01	4978–5285
OS-136223*	417.5	$4040 \pm 25$	<63 µm bulk peat	-25.6	1	-
OS-126728	422.5	$4540 \pm 25$	<63 µm bulk peat	-26.5	0.02	5053-5315
OS-126794*	422.5	$4880 \pm 20$	Mangrove wood	-27.2	1	-
OS-130981	437.5	$4530 \pm 20$	<63 µm bulk peat	-27.2 $-27.3$	0.03	5052–5310
OS-136224*	442.5	$3340 \pm 25$	<63 μm bulk peat	-24.3	1	
OS-130224 OS-129583	454.5	$4830 \pm 25$	Mangrove wood	-24.3 -27.1	0.01	- 5478–5598
OS-129565 OS-130671	464.5	$4940 \pm 25$	Mangrove wood	-28.1	0.01	5598–5718
OS-130071 OS-129577*	485.5	$4180 \pm 25$	<63 μm bulk peat	-26.1 $-26.3$	1	-
OS-129377 OS-130982*	487.5	$4050 \pm 20$	<63 μm bulk peat	-25.8	1	_
OS-130982 OS-126729*	489.5	$3600 \pm 20$	<63 μm bulk peat	-23.8 -24.1	1	_

<sup>&</sup>lt;sup>\*</sup> Sample with >95% outlier probability (estimated by Bchron age-depth model) and excluded from further analysis.

across the database and those that are confined to smaller regions; and (3) a hyperparameter level, which characterizes prior expectations regarding dominant spatial and temporal scales of RSL variability.

At the data level, we observe noisy RSL  $y_i$  and noisy age  $t_i$ :

$$y_i = f(\mathbf{x}_i, t_i) + \epsilon_i^y + w(\mathbf{x}_i, t_i) + y_0(\mathbf{x}_i)$$
 (2)

$$t_i = \hat{t_i} + \epsilon_i^t \tag{3}$$

where  $x_i$  and  $t_i$  are the geographic location and true age, respectively, of observations indexed by i;  $f(x_i, t_i)$  is the true RSL value at  $x_i$  and  $t_i$ ;  $e_i^Y$  is the vertical error of each RSL data point (assumed to be independent and normally distributed);  $w(x_i, t_i)$  is a supplemental white noise term that accounts for variations in the data that cannot be explained by the terms in the process-level model;  $y_0(x_i)$  is a site-specific datum offset to ensure that RSL data can be directly compared.  $\hat{t}_i$  is the mean estimated age of each RSL data point and  $e_i^t$  is its error. The age uncertainties are incorporated using the noisy-input Gaussian Process (GP) method of McHutchon and Rasmussen (2011), which uses a first-order Taylor-series approximation to translate errors in the independent variable into equivalent errors in the dependent variable:

$$f(\mathbf{x}_i, t_i) \approx f(\mathbf{x}_i, \widehat{t}_i) + \epsilon_i^j \frac{\partial f(\mathbf{x}_i, \widehat{t}_i)}{\partial t}$$
 (4)

At the process level, we model the sea-level field,  $f(x_bt_i)$ , as the sum of two component fields, f(x,t) = r(t) + l(x,t) where x represents geographic location and t represents time. The two components are: a common regional term, r(t), representing the time-varying signal shared by all sites included in the analysis, and a local term, l(x,t), which represents site-specific processes. The priors for each term in the model are mean-zero Gaussian processes (Rasmussen and Williams, 2006) with 3/2 Matérn covariance functions (see Ashe et al., 2019 for more details). Hyperparameters defining prior expectations of the amplitudes and spatio-temporal scales of variability were estimated through maximum-likelihood optimization (Table 5; Table S3).

We ran sensitivity tests to assess the robustness of the local signal to alternative model structures and input data (Table S3; Fig. S2). These tests included 1) using only the new Swan and Snipe records as input data (CrL-SS); 2) changing the common regional term to one that varies spatially with a zero-mean prior (RL) or a GIA prior (RL-GIA); and 3) adding an additional spatially varying term to the model (CrRL). These tests demonstrate that the local signal is relatively insensitive to model

**Table 4**Radiocarbon ages from core SBC10.

Sample ID	Depth (cm)	<sup>14</sup> C age (years)	Dated material	$\delta^{13}$ C (‰)	Outlier probability (%)	2σ-calibrated age range (cal a BP)
OS-134377	33.5	$105\pm20$	Mangrove wood	-26.6	0.01	30–258
OS-132811	50.5	$350\pm15$	Mangrove wood	-24.2	0.02	319-474
OS-134378*	67.5	$165\pm15$	Mangrove wood	-24.5	0.99	_
OS-132812	77.5	$1030\pm20$	Mangrove wood	-27.0	0.01	920–956
OS-134336	91.5	$1140\pm15$	Mangrove wood	-24.9	0.01	974–1173
OS-132813	98.5	$1110\pm15$	Mangrove wood	-26.1	0.02	959–1057
OS-132814	107.5	$1530\pm25$	Mangrove wood	-25.0	0.01	1349–1514
OS-134379	126.5	$1720\pm20$	Mangrove wood	-26.6	0.01	1545–1696
OS-129823	145.5	$1800\pm15$	<63 µm bulk peat	-24.8	0.01	1627-1733
OS-134337	159.5	$1700\pm15$	Mangrove wood	-26.8	0.03	1541–1689
OS-133069	178.5	$2150\pm20$	<63 µm bulk peat	-25.3	0.01	2008-2298
OS-134690	191.5	$2330\pm20$	<63 µm bulk peat	-26.4	0.15	2331-2358
OS-133066	211.5	$2160\pm15$	<63 µm bulk peat	-25.6	0.01	2069-2299
OS-134574	236.5	$2350\pm25$	<63 µm bulk peat	-25.7	0.01	2333-2462
OS-129771	250.5	$2500\pm20$	Mangrove wood	-25.3	0.01	2494–2721
OS-134380	261.5	$2580\pm30$	Mangrove wood	-26.5	0.01	2521-2758
OS-132815	278.5	$2790\pm20$	Mangrove wood	-25.0	0.01	2805-2957
OS-134691	297.5	$2940\pm20$	<63 µm bulk peat	-27.0	0.01	3004-3164
OS-132816	318.5	$2970\pm20$	Mangrove wood	-25.7	0.01	3069-3210
OS-134692	330.5	$3180 \pm 25$	<63 µm bulk peat	-26.6	0.01	3365-3448
OS-129824	349.5	$3550\pm20$	Mangrove wood	-27.0	0.12	3725-3901
OS-134338	361.5	$3470\pm20$	Mangrove wood	-25.9	0.01	3647-3829
OS-132817	382.5	$3350\pm20$	Mangrove wood	-27.0	0.89	3491-3682
OS-134381	394.5	$3600\pm30$	Mangrove wood	-27.8	0.01	3781-4058
OS-133068	415.5	$3870\pm20$	<63 µm bulk peat	-26.1	0.02	4164-4408
OS-134575	439.5	$3830\pm20$	<63 µm bulk peat	-25.6	0.03	4103-4352
OS-129772	455.5	$4260\pm25$	Mangrove wood	-26.6	0.06	4732-4864
OS-134382	473.5	$4250\pm25$	Mangrove wood	-27.0	0.01	4657-4861
OS-132818	490.5	$4410\pm25$	Mangrove wood	-26.3	0.01	4868-5230
OS-132819*	515.5	$5230\pm25$	Mangrove wood	-27.0	1	_
OS-134576	532.5	$4650\pm20$	<63 µm bulk peat	-27.0	0.01	5316-5462
OS-129825*	548.5	$5290\pm20$	Mangrove wood	-27.7	1	_
OS-134693	568.5	$4960\pm25$	<63 µm bulk peat	-27.7	0.01	5602-5732
OS-134577*	588.5	$5360\pm20$	<63 µm bulk peat	-26.6	1	_
OS-133067*	614.5	$4520\pm20$	<63 µm bulk peat	-26.3	1	_
OS-134383*	630.5	$5490\pm20$	Mangrove wood	-27.4	1	_
OS-129826	648.5	$5000\pm20$	Mangrove wood	-28.7	0.01	5610-5881
OS-134339	657.5	$5120\pm25$	Mangrove wood	-28.1	0.01	5754–5929
OS-132820	676.5	$5230\pm25$	Mangrove wood	-27.1	0.01	5920–6167
OS-134384	691.5	$5380 \pm 30$	Mangrove wood	-29.7	0.01	6009–6281
OS-132821	714.5	$5340 \pm 25$	Mangrove wood	-29.6	0.01	6003–6265
OS-134385*	731.5	$3580 \pm 20$	Mangrove wood	-28.6	1	_
OS-129827	750.5	$5370 \pm 20$	Mangrove wood	-26.9	0.01	6009–6276

<sup>\*</sup> Sample with >95% outlier probability (estimated by Bchron age-depth model) and excluded from further analysis.

structure, and our chosen model (CrL; Figs. 5, 6, 7; Fig. S2; Table S3) is the most parsimonious and best performing.

The optimized values indicate that the largest signal comes from the common regional term, which has a prior standard deviation of  $\pm 5.6$  m and a decorrelation timescale of 3.9 ka (Fig. 7D). The local term contributes  $\pm 0.2$  m with a decorrelation timescale of 2.1 ka and a decorrelation length scale of  $\sim 3$  km. The supplemental white noise term is small ( $\sim 1$  cm), indicating that the stated measurement uncertainties are adequate to explain the difference between the process model and the proxy data observations. The output of the model includes an estimate of the posterior probability distribution of the sea-level field, f(x,t), conditional on the tuned hyperparameters and the data. The reported rates of sea-level change are 100-year average rates based on a linear transformation of f(t), and model predictions are expressed as the mean and  $1\sigma$  uncertainty, unless otherwise stated.

Our new mangrove reconstructions indicate that the sites experienced different RSL changes during the past  $\sim$ 5 ka, with a faster millennial-scale rate of rise occurring at Swan Key compared to Snipe Key (Fig. 5). To better understand which site (if any) was more/less representative of regional-scale RSL trends, we used the STEHM to place the new reconstructions into a wider geographic and temporal context (Fig. 7). Decomposition of the full RSL signal by the STEHM attributes  $\sim$ 1 m of RSL rise at Swan Key to local-scale processes during the past  $\sim$ 5 ka (Fig. 5). Importantly, our near-continuous RSL reconstruction from

Swan Key is compatible with index points derived from Robbin (1984) at the same site (Fig. 7C). This result indicates that both studies are likely representative of RSL at the site and the RSL reconstructions are reproducible within a site (among cores).

#### 4. Discussion

## 4.1. Near-continuous RSL reconstructions from mangrove sediment

The Atlantic coast of North America has the greatest number and highest density of near-continuous, late Holocene RSL reconstructions, and these records were generated exclusively from sequences of salt-marsh sediment (Fig. 1A). The success of this approach arises because long-term, GIA-driven RSL rise (e.g., Peltier, 1996) created accommodation space that was filled by in-situ, organic sediment with a high concentration of recognizable plant macrofossils and microfossils that grew immediately below (e.g., rhizomes), or on (e.g., foraminifera), paleo marsh surfaces. Plant macrofossils are ideal specimens for radiocarbon dating paleo marsh surfaces (e.g., Kemp et al., 2013b), and the preservation of foraminifera enables the tidal elevation of those surfaces to be quantitatively reconstructed (e.g., Horton and Edwards, 2005; Kemp and Telford, 2015). Ongoing burial reduces bioturbation from the typically small and shallow roots of salt-marsh plants and promotes preservation by introducing paleomarsh surfaces to anoxic conditions as

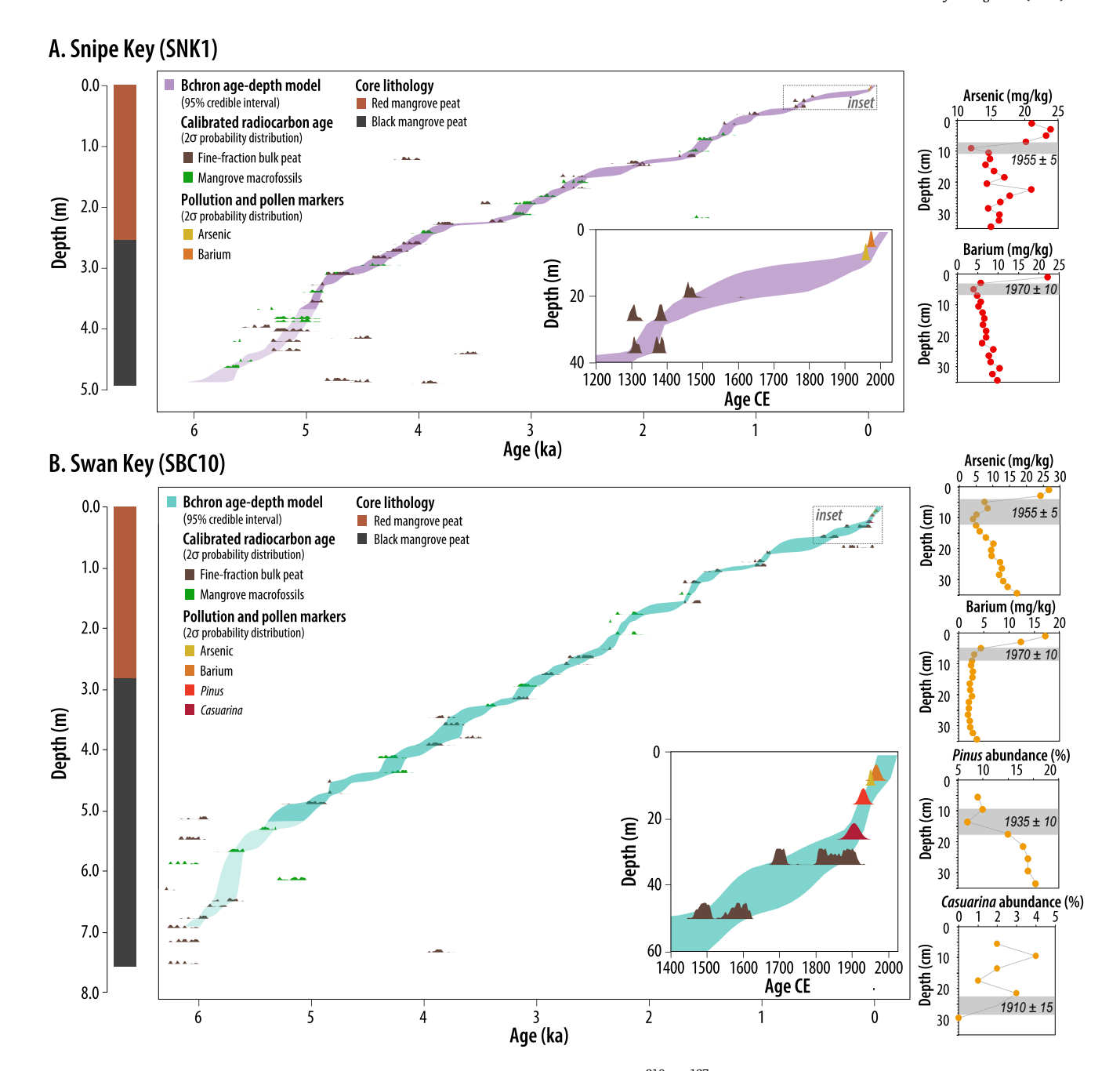


**Fig. 4.** Core chronologies from (A) Snipe Key (B) and Swan Key. Downcore profiles of As, Ba, <sup>210</sup>Pb, <sup>137</sup>Cs, and *Pinus* and *Casuarina* pollen abundance for cores SNK1 (red circles) and SBC10 (yellow circles). Shaded depth intervals indicate each horizon (and sampling uncertainty), and the labeled ages show its assigned age (and uncertainty) included in the age-depth model. Radiocarbon ages and the probability distribution of the 2σ calibrated age range are shown in dark purple (SNK1) and green (SBC10). The shaded envelopes show the 95% credible interval of the Bchron age-depth model. (For interpretation of the references to color in this figure legend, the reader is referred to the web version of this article.)

sediments accumulate over time (e.g., Niering et al., 1977).

Mangroves replace salt marshes in warmer regions and become the dominant ecosystem in low-energy, intertidal environments (Saintilan et al., 2014). Therefore, mangrove peat has been used to produce index points in much the same way as salt-marsh peat (e.g., Ellison, 1993; Toscano and Macintyre, 2003; Woodroffe et al., 2015a). However, developing near-continuous, late Holocene RSL reconstructions from sequences of mangrove peat has proven challenging, primarily for two reasons. First, foraminifera are subject to poor or selective preservation in buried mangrove sediment (Berkeley et al., 2009; Khan et al., 2019), despite being observed to form elevation-dependent groups of calcareous and agglutinated taxa in surface sediment from analogous modern

environments (Horton et al., 2003, 2005; Woodroffe et al., 2015a). We used sediment lithology as a sea-level proxy and a classification approach that treated elevation as a discrete variable by recognizing that mangrove peat formed between MTL and HOP with the highest probability of formation halfway between these points. This approach constrained the elevation of paleomangrove surfaces to within  $\pm 0.23$  m at Snipe Key and  $\pm$  0.19 m at Swan Key (1 $\sigma$ ),  $\sim \! 56\%$  of tidal range at each site. This vertical resolution is likely sufficient to make meaningful inferences about late Holocene RSL change in South Florida. However, the precision of this approach is a function of tidal range, thus in regions with larger tidal ranges, reconstruction uncertainty would be correspondingly larger. Therefore, in the absence of foraminifera, it is

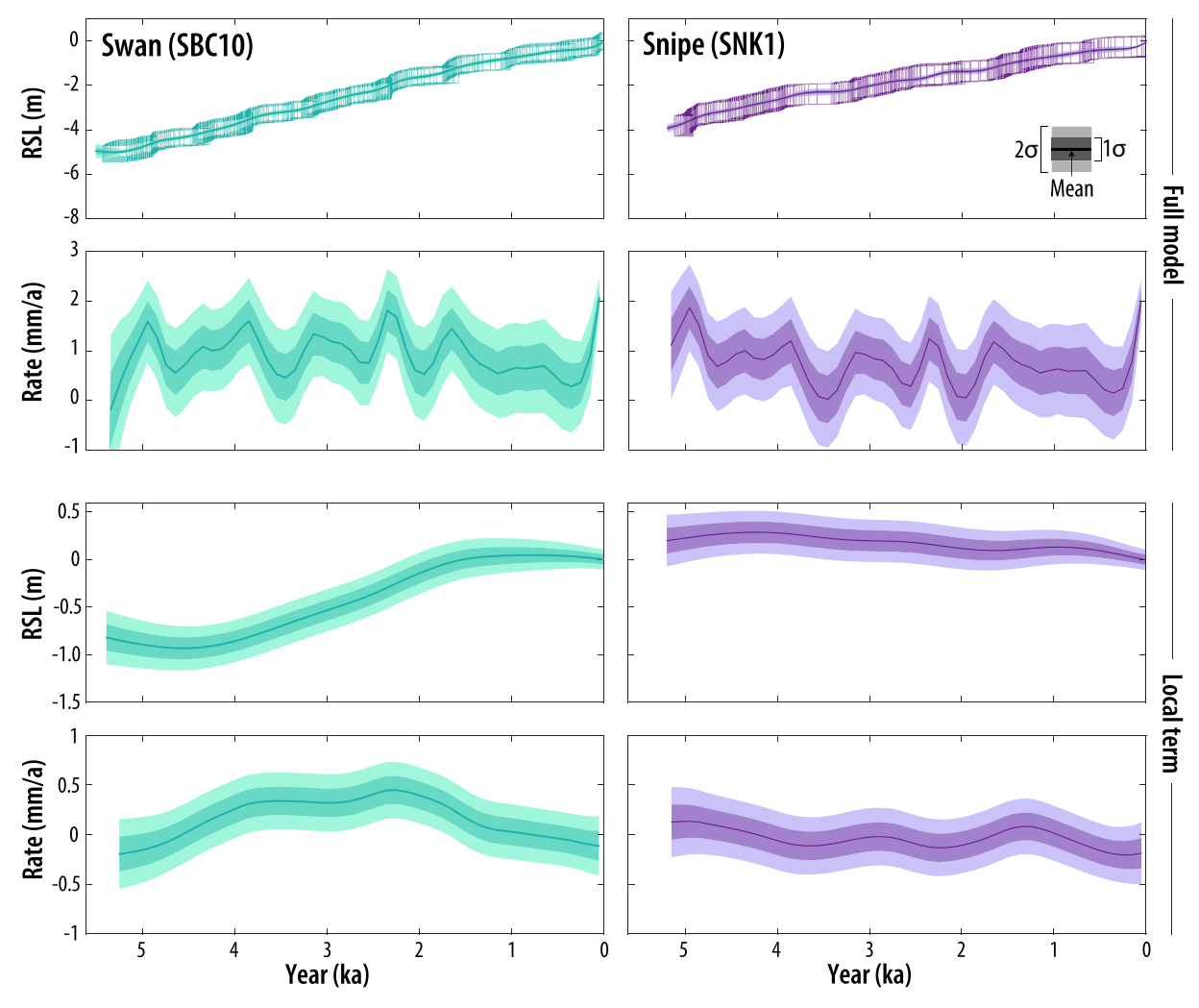
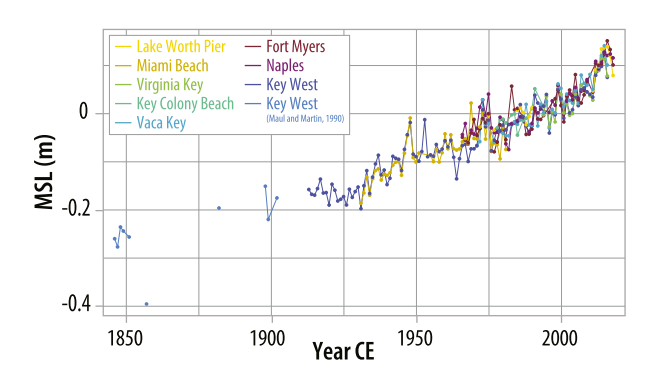


Fig. 5. (A) Relative sea-level (RSL) reconstructions from Snipe Key and Swan Key and the decomposition of local signals from these records using the spatio-temporal statistical model. For all plots, the model mean and  $1\sigma/2\sigma$  uncertainty are represented by a solid line and shaded envelopes.



**Fig. 6.** Annual mean sea level (MSL) recorded by tide gauges in South Florida. Data were downloaded from NOAA NOS Center for Operational Oceanographic Products and Services or the Permanent Service for Mean Sea Level (PSMSL). The Key West tide-gauge record is extended by the addition of archival data recovered and presented by Maul and Martin (1993).

particularly important that efforts to produce detailed RSL reconstructions using classification of sediment type focus on regions with small tidal range. Indeed, even in cores of salt-marsh peat with excellent preservation and abundant foraminifera, some studies in regions of exceptionally small tidal range opted to use a classification approach because the accuracy and precision of the reconstruction was not improved by using more complex methods such as transfer functions that treat elevation as a continuous variable (e.g., Barlow et al., 2013; Kemp et al., 2014, Kemp et al., 2017b).

The second challenge associated with developing near-continuous RSL reconstructions from mangrove archives is that their radiocarbon chronologies often exhibit ages out of stratigraphic order and differences in sample age depending on the material dated, and it is often unclear how dated materials (e.g., roots) relate to paleomangrove surfaces (Ono et al., 2015; Punwong et al., 2013; Woodroffe et al., 2015a; Sefton et al., 2022). These issues likely arise, at least in part, from the size and depth reached by the roots of mangrove trees that cause physical bioturbation and deepen the oxic zone in sediment, which is often compounded by a lack of long-term RSL rise to create accommodation space. The lowlatitude regions where mangroves exist are commonly far-field sites with respect to the distribution of ice sheets at the Last Glacial Maximum (Clark et al., 1978; Peltier, 2004; Khan et al., 2015; Saintilan et al., 2020). Far-field sites typically experienced RSL fall from a mid-Holocene highstand (or minimal rise). Under this background regime of RSL change, accommodation space is not created and paleomangrove surfaces are not buried, resulting in prolonged exposure to oxic conditions and higher likelihood of physical reworking.

Radiocarbon dates in both cores showed stratigraphic ordering within and among different dated materials (e.g., fine-fraction bulk peat or macrofossils; Fig. 4; Fig. S3). This result suggests that reliable chronologies can be obtained from near-continuous sequences of mangrove

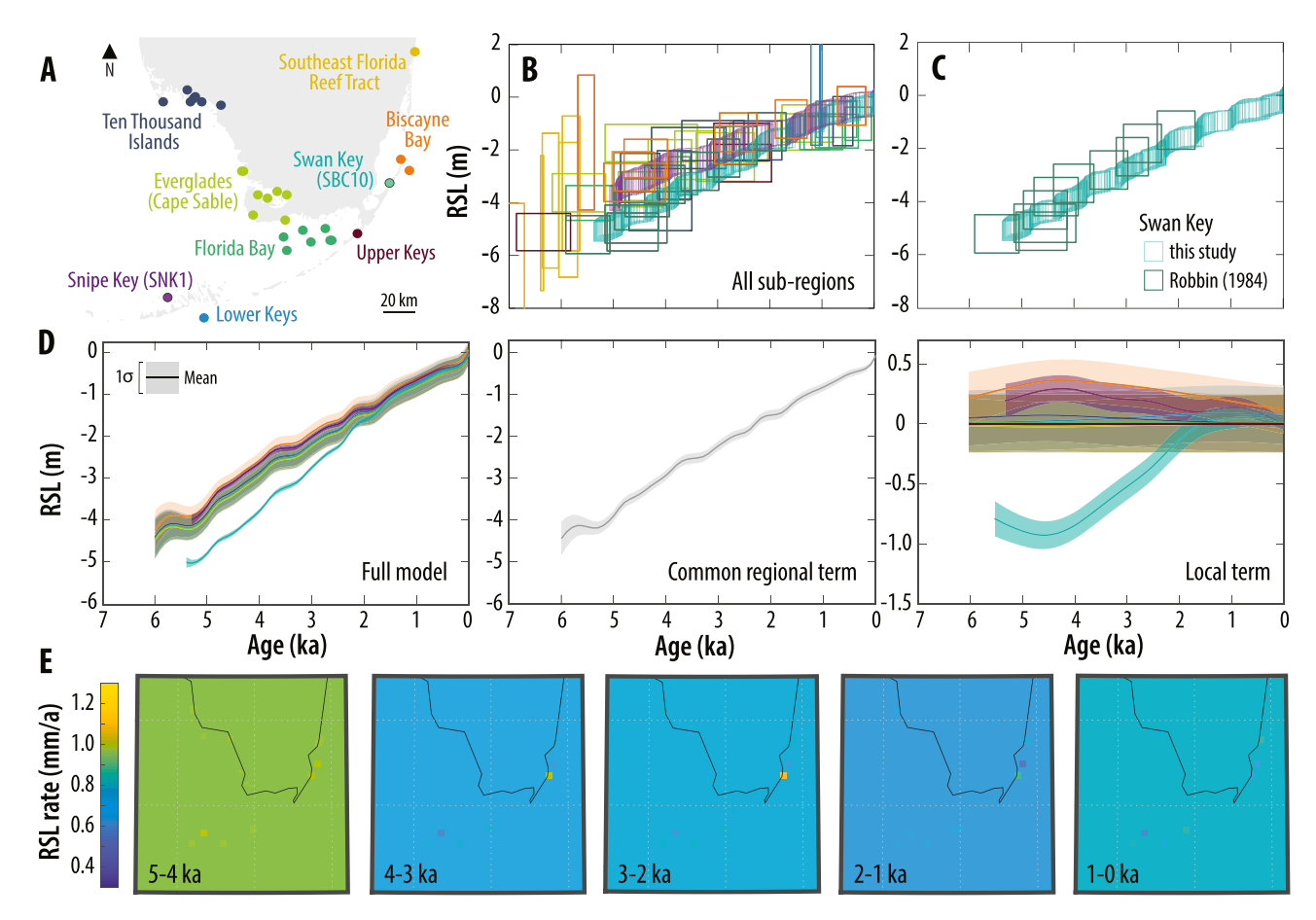


Fig. 7. Comparison of the new relative sea-level (RSL) reconstructions from SNK1 and SBC10 to existing sea-level data from mangrove and coral indicators in South Florida. (A) Location of index points from the South Florida database. (B) Sea-level index points (depicted as boxes) for all sub-regions in South Florida, including data from an earlier study by Robbin (1984) at Swan Key (C). The color of each index point and model estimate corresponds to the colored circles which denote their location/sub region on the site map (B). (D) Decomposition of the spatio-temporal statistical model applied to the regional dataset, where the mean (solid line) and shading ( $1\sigma$  uncertainty) for each of the sub regions are shown. (E) Spatial patterns in rates of RSL change in South Florida estimated from the spatio-temporal statistical model over 1000-year intervals for the past 6 ka.

**Table 5**Optimized hyperparameters for the spatio-temporal empirical hierarchical model.

Term	Prior standard deviation (m)	Characteristic timescale (ka)	Characteristic length scale (degrees)			
r(t) [common regional]	$\pm$ 5.6	3.9	-			
$l(\mathbf{x},t)$ [local]	$\pm~0.2$	2.1	0.01			
<pre>w(x,t) [additional   uncertainty]</pre>	$\pm~0.01$	-	-			
$y_0(t)$ [site-specific offset]	$\pm~0.0$	-	_			

peat by radiocarbon dating several types of subsamples and that these sample types can be reasonably combined with one another to produce a chronology of sediment accumulation. Agreement between ages from macrofossils and bulk sediment suggests that the carbon fractions removed through base washing are not systematically different in age to other carbon fractions in the peat matrix, which has been observed in other Holocene radiocarbon dating applications (e.g., Wild et al., 2013). The robust chronologies from South Florida likely reflect a somewhat unusual set of circumstances where mangroves are present in a region experiencing long-term RSL rise from ongoing GIA subsidence. South Florida is an intermediate- rather than far-field site because of its location on the collapsing forebulge of the Laurentide Ice Sheet (e.g., Peltier,

2004; Milne et al., 2005; Love et al., 2016). Without this mechanism for creating accommodation space, it is possible that a reliable, stratigraphically-ordered chronology could not have been obtained.

We conclude that mangrove peat in South Florida is a viable source of near-continuous, late Holocene RSL reconstructions due to the combination of a small tidal range and background trend of RSL rise. Where similar conditions exist, we propose that RSL reconstructions of comparable resolution could be successfully generated from mangrove peat. Sites in Bermuda (e.g., (Ellison, 1993; Kemp et al., 2019), Central America (e.g., Belize, Panama, and Honduras; McKee et al., 2007; Cahoon et al., 2003), and the Caribbean (e.g., Ramcharan and McAndrews, 2006; Woodroffe, 1981) are known to have thick sequences of mangrove peat that accumulated under conditions of GIA-driven RSL rise. Even in far-field regions predicted to experience late Holocene RSL fall, it is possible that some localities experienced (for example) linear tectonic subsidence with sufficient magnitude to cause net RSL rise (e.g., Bloom, 1970; Ellison and Strickland, 2015; Kelsey, 2015). Such locations are candidates for developing near-continuous RSL reconstructions from mangrove peat to expand the geographic distribution of records.

# 4.2. Within-region replication of RSL reconstructions

We reconstructed RSL at two sites to distinguish the influence of local and regional-scale processes on RSL in South Florida. Previous studies of late Holocene RSL change in the western North Atlantic Ocean typically emphasized RSL variability among regions by reconstructing RSL at single sites spaced far from other reconstructions (e.g., Kemp et al., 2011, 2014; Gehrels et al., 2020). Given the growing number and density of near-continuous RSL reconstructions along the Atlantic coast of North America, investigations of within-region (and within-site) variability are increasingly important to gauge the robustness of reconstructed local and regional patterns of RSL change and their attribution to specific physical processes (e.g., Barlow et al., 2013; Kemp et al., 2017b, 2018; Bush et al., 2020). For example, GIA modeling studies often use RSL data for model tuning and validation; RSL records with substantial unrecognized influence from local-scale processes may bias comparisons to model predictions (e.g., Garrett et al., 2020).

There are several lines of evidence to suggest that Snipe and Swan Key (~160 km apart; Fig. 1) should share common RSL trends in the absence of significant local effects. Tide gauges in South Florida measure spatially-coherent RSL trends on annual to multi-decadal timescales (Fig. 6), with no discernible difference between trends at Key West and Vaca Key (closest to Snipe Key) and those at Miami Beach and Virginia Key (closest to Swan Key). Piecuch et al. (2018) combined tide-gauge measurements, a database of proxy RSL reconstructions, continuous global positioning satellite measurements, and a suite of Earth-ice model predictions to estimate multi-decadal to century-scale trends in RSL and vertical land motion. In that analysis, the difference in trend between Snipe Key and Swan Key is  $-0.1 \pm 1.2$  mm/a (median  $\pm$  95% credible interval) for RSL, 0.0  $\pm$  1.1 mm/a for vertical land motion, and 0.0  $\pm$ 0.6 mm/a for sea surface height. On multi-centennial to millennial timescales, most Earth-ice model pairings predict no meaningful RSL difference between Snipe Key and Swan Key (Fig. 1B). Those predictions that do, estimate higher RSL at Swan Key compared to Snipe Key by as much as 0.8 m (Fig. S4), opposite the pattern we reconstructed. Finally, predictions of how Mississippi Delta loading influences RSL rise through subsidence and distortion of the geoid indicate that Snipe Key and Swan Key are far enough away to experience no effect from these processes (e. g., Wolstencroft et al., 2014; Kuchar et al., 2018). These lines of evidence suggest no a priori expectation that the two study sites should experience and record different RSL histories.

# 4.3. Drivers of local RSL change

The reproducibility of RSL records at Swan Key (Fig. 7C) demonstrates that the site's apparently anomalous RSL history does not arise from the approaches used, but rather that the site is influenced by physical process(es) acting at local scales over millennial timescales.

Sediment compaction of shallow and deeper strata contributes to variable rates of land subsidence that cause PDL of the sediment used to reconstruct RSL and subsequently results in overestimation of the amount and rate of RSL rise (e.g., Bloom, 1964; Kaye and Barghoorn, 1964; Brain et al., 2011, 2017). Our quantitative estimates of PDL through sediment autocompaction indicate that it cannot be reasonably invoked as a significant local-scale process. We estimate PDL of the samples used to reconstruct RSL to be approximately two orders of magnitude smaller than the difference in RSL between Snipe Key and Swan Key (Figs. 3, 5). Furthermore, geotechnical analysis of another core of mangrove peat collected at Swan Key led Toscano et al. (2018) to similarly conclude that compaction of late Holocene strata at the site was minimal, which demonstrates that different approaches to estimating PDL produce similar results and thus are likely robust.

Groundwater withdrawal can accelerate subsidence by reducing porewater pressure, which leads to compression and reduced volume of subsurface sediment units (e.g., Dixon et al., 2006; Kolker et al., 2011; Karegar et al., 2016; Johnson et al., 2018). Depending on the underlying aquifer and geological structures, the resulting subsidence can manifest at local to regional scales. However, groundwater withdrawal is unlikely to be the cause of the RSL difference between Swan Key and Snipe Key for (at least) four reasons. First, there is no pumping at the site, so any contribution would be part of a regional trend (and therefore common to both sites and others analyzed in the spatio-temporal model). Second,

both study sites are likely sufficiently distal to areas of active pumping in the Biscayne aquifer (e.g., Miller, 1990) to directly be impacted by this effect. Third, if the 1-m RSL difference between Swan Key and Snipe Key is caused by recent (i.e., 20th century) groundwater withdrawal, there would be a pronounced difference in the rate of modern RSL rise, for which there is no evidence from proxy reconstructions (Fig. 5), tide gauges (Fig. 6), or space geodetic constraints (Peltier et al., 2015). Fourth, the effect of groundwater withdrawal in karst systems is instantaneous adjustment through sink hole collapse rather than the gradual process that is observed in non-carbonate systems (e.g., Lamoreaux and Newton, 1986; Waltham and Fookes, 2003). This temporal trend is in contrast to the prolonged contribution inferred from spatio-temporal modeling.

Isostatic uplift induced by karstic mass loss has been proposed as a mechanism to explain regional-scale RSL change over million-year time scales (e.g., Opdyke et al., 1984; Adams et al., 2010; Creveling et al., 2019), but localized carbonate weathering at the base of sedimentary sequences has received less scrutiny as a mechanism to explain local subsidence. The acidity of mangrove peat can dissolve underlying carbonate at the bedrock-peat contact, causing shallow depressions in limestone to become deeper (Zieman and Joseph, 1972; Odum et al., 1982). Mangroves in the depression must fill the newly-created accommodation space to maintain their position in the tidal frame. Dong et al. (2018) identified 1.5 to 2-m deep, 80 to 200-m diameter depressions in limestone bedrock beneath wetlands in the Big Cypress National Preserve (Fig. 1b). They used a reactive-transport kinetics model to estimate that the depressions likely formed within the past 9.5 ka and deepened at ~0.1-0.4 mm/a over this time. Similarly, Chamberlin et al. (2018) and Zhang et al. (2019) estimated the development of these depressions began in the early to mid Holocene at rates consistent with those suggested by Dong et al. (2018) based on radiocarbon dating of wetland sediments and weathering rates constrained by mass balance of calcium and phosphorous.

Stratigraphic investigations show that the cores from Swan and Snipe Keys were collected from depressions in limestone bedrock (Fig. 1). The depression at Snipe Key is elongate and extends a considerable distance along the Snipe Keys chain (Fig. 1), suggesting that the mangrove islands formed in a pre-existing tidal channel, rather than in a local dissolution basin. In contrast, the core from Swan Key was collected from a bedrock depression with morphology that is analogous to those found in Big Cypress reserve. Furthermore, the lithology of the Key Largo coralline limestone bedrock underlying Swan Key is more porous and prone to weathering than the oolitic Miami Limestone that underlies Snipe Key (Hickey et al., 2010; Harris et al., 2018). This contrasting morphology and lithology of underlying carbonate could support a hypothesis that the enhanced rate of RSL rise at Swan Key (as compared to Snipe Key and the wider region) arises from carbonate dissolution. The estimated rate of deepening (~0.1-0.4 mm/a; Dong et al., 2018; Chamberlin et al., 2018) is similar to the difference in RSL rise between Snipe Key and Swan Key, and furthermore, it is likely to be a process that occurred throughout the late Holocene rather than being initiated recently (e.g., groundwater withdrawal) or acting sporadically (e.g., sink hole creation). Moreover, Dong et al. (2018) found a relationship between soil thickness and maximum weathering rate (reached at thicknesses of 1.5 to 2 m), which could explain the enhanced rates of the local process observed at Swan Key (Fig. 5) as the peat column reached and then exceeded this thickness between 4 and 2 ka. However, given that limestone weathering rates are controlled by complex interactions among soil thickness, climate, and local hydrologic and biotic processes (Dong et al., 2018), further investigation is ultimately needed to evaluate if conditions at Swan Key could sustain equivalent weathering rates to those estimated at Big Cypress. This could be achieved empirically through reconstructing RSL using other cores from outside of the bedrock depression along the stratigraphic transect that we investigated (Fig. 1f). Importantly, this mechanism of local-scale RSL change is (at least along the Atlantic coast of North America) restricted to South

Florida because karst bedrock is not present elsewhere and it cannot therefore be invoked to explain local-scale differences at sites in New England, for example. As such, reconstructed differences in RSL among closely-spaced sites in South Florida do not necessarily indicate that late Holocene RSL reconstructions more widely fail to exhibit within-region reproducibility.

Another local-scale process to consider is non-stationarity of Holocene tides. Modeling of Holocene tides along the U.S. Atlantic and Gulf of Mexico coasts suggests that tidal range was largely unchanged at regional scales during the last ~7.0 ka (Hill et al., 2011), and the influence on the distribution of mangrove and coral sea-level indicators in South Florida and the greater Caribbean region over this time was small (<0.15 m; Khan et al., 2017). However, the paleo-bathymetric resolution of the Hill et al. (2011) paleo-tidal model cannot accurately estimate local-scale variations in paleo tidal range (e.g., Hall et al., 2013; Hawkes et al., 2016). Given the geomorphic setting (i.e., absence of complex barrier/inlet systems and connection to the open ocean), it is unlikely that the influence of non-stationary tides was considerable, although incorporating higher-resolutionpaleogeographies into paleotidal models may ultimately help to resolve the impact of this process on South Florida RSL reconstructions.

A final consideration to explain the difference between the Swan and Snipe records is the indicative meaning we assumed in our approach. First, the conservative indicative meaning we used in our sediment classification approach did not divide peat-forming mangroves into more precise sub-zones. For example, it is possible that mangroves at Snipe Key maintained a higher position in the intertidal zone and accumulated peat at a rate consistent with RSL rise (i.e., PME was constant over the period of accumulation). In contrast, mangroves at Swan Key may have initiated at a lower PME within the indicative range (e.g., close to MTL) and over time the rate of peat accumulation was greater than RSL rise (i.e., emergence). Alternatively, if Snipe Key experienced submergence with constant PME at Swan Key, the effect would be the same. Given the indicative range of peat-forming mangroves at each site ( $\pm$  0.46 m at Snipe Key and  $\pm$  0.37 m at Swan Key), this scenario could explain  $\sim$ 30–40% of the apparent 1-m difference in RSL between the two sites and also account for its decrease over time. A number of factors, such as resource availability (e.g., nutrients, space, and light), stressor gradients (e.g., salinity, nutrients), and sediment delivery can interact with RSL changes to influence productivity and accretion in mangroves (Lugo and Snedaker, 1974; Rovai et al., 2018; Rivera-Monroy et al., 2019). Jones et al. (2019) proposed that a period of frequent storms and prolonged drought in the late Holocene resulted in rapid transgression across Florida Bay at ~3.4-2.8 ka as mangroves transitioned to estuarine environments. This observation is further supported by geochemical profiles from Shark River Estuary in the Everglades, which indicated a period of intense hurricane activity at  $\sim$ 3.4–3.0 and  $\sim$ 2.2–1.5 ka (Yao et al., 2020). However, these mechanisms are related to regional-scale climate variability, and presumably would influence both sites. Indeed, at both sites, very low accumulation rates are observed between  $\sim$ 3.4–3.2 and  $\sim$ 2.0–1.7 ka. Furthermore, the timing of these climatic changes is inconsistent with when the largest differences in the Snipe and Swan Key records are observed between ~5-3 ka. Therefore, this explanation cannot fully reconcile the differences between the sites and still requires at least a moderate contribution from a local process acting over at least the past 5 ka.

Relatedly, it is possible that increased salinity in Biscayne Bay during the 20th century could have placed stress on mangroves, resulting in decreased production and accretion, and causing mangroves to form at progressively lower elevations during the 20th century. However, this seems to be unlikely given that core SBC10 was collected nearby to the elevation apex of the island close to HAT (thus occurring towards the top, rather than bottom of the range) and the age-depth model suggests an increase (rather than decrease) in sedimentation rate over this time interval. Furthermore, Snipe Key also exhibited a rapid 20th century RSL rise, but under contemporary conditions, Snipe Key's location in the

backcountry of the Florida Keys is not strongly influenced by changes in outflows through the Everglades and western Florida Bay because they tend to follow a trajectory where they exit to south of the Keys through channels in the Middle Keys and therefore do not reach the backcountry (Smith, 1994; Boyer and Jones, 2001).

A second potential issue with the indicative meaning we assumed in our approach is the possibility that some sections of the cores that suffered from poor preservation of foraminifera may actually have formed under freshwater conditions at an elevation higher than the indicative meaning we estimated for mangroves. This may particularly be the case at Swan Key due to its greater connection to freshwater outflows from the Everglades, which would likely have been enhanced in the mid to late Holocene when RSL was lower (McPherson and Halley, 1996). Although patchy towards the base of the core, foraminifera were preserved at all depths of core SNK1, whereas core SBC10 suffered from lack of preservation below 3 m in depth (Table S2). Although wood and roots preserved in SBC10 suggest a mangrove origin (a conclusion also obtained by Robbin, 1984), it is possible for mangrove roots to penetrate to deeper depths, complicating the identification of mangrove peats on the basis of plant macrofossils alone. However, if the base of SBC10 did include freshwater peat, this would exacerbate the difference in reconstructed RSL at Swan and Snipe Keys because the indicative meaning of freshwater peat could potentially be higher than that of mangroves, resulting in lower reconstructed RSL. Furthermore, any potential bias introduced would likely be small. Peat-forming freshwater vegetation communities in the Everglades found in close association with mangroves occur at low elevations comparable to the elevation distribution of mangroves (Fig. S5). Given the bathymetry of the Florida shelf and the proximity of Swan Key to the steep shelf slope, it seems unlikely that this location would have been very far inland from the paleo shoreline as the shelf was flooded. Therefore, higher elevation, inland peat-forming freshwater environments are likely not a good analogue for conditions at Swan Key. This suggests that if SBC10 did include peat that accumulated under freshwater influence (but in close association with mangroves), the potential bias introduced in the interpretation of the indicative meaning of the cores would likely be small.

# 5. Conclusions

We produced the first near-continuous records of RSL change from mangrove archives for the past 5 ka from two cores collected from Snipe and Swan Keys in South Florida. From site surveys and remote sensing analysis, we corroborated the putative indicative meaning of mangrove indicators and demonstrate that they form within a normal distribution approximately between MTL and HAT. Due to poor preservation of foraminifera in the cores, we adopted a conservative indicative meaning of MTL to HOP (2σ distribution) for undifferentiated mangrove peat recovered in cores, a range likely large enough to encompass all species of mangrove and their geomorphic settings in South Florida. We also outlined an approach to produce accurate chronologies from mangrove archives by dating mangrove macrofossils (where present) and the fine fraction of bulk peat in the absence of macrofossils. Radiocarbon dates in both cores were in stratigraphic order regardless of the material dated, which suggests that reliable chronologies can be obtained from nearcontinuous sequences of mangrove peat by dating several types of subsamples. We show that mangrove peat can provide detailed RSL reconstructions in microtidal regions that have undergone long-term RSL rise, even in cases where foraminifera are poorly preserved. We suggest that in locations where similar conditions persist, mangrove peat should provide reconstructions of comparable resolution to those presented

During the past  $\sim$ 5 ka, RSL rose at Snipe Key by 3.7 m (average of  $\sim$ 0.75 mm/a), compared to 5.0 m at Swan Key (average of  $\sim$ 1.0 mm/a). At both sites, the rate of RSL rise since  $\sim$ 1900 CE ( $\sim$ 2.1 mm/a) is the fastest during the past  $\sim$ 5 ka. We used a spatio-temporal model to decompose trends from RSL reconstructions from a network of sites

across South Florida to quantify regional- and local-scale signals. This analysis demonstrated that Snipe Key was representative of regional-scale trends, but that Swan Key experienced RSL rise that included a substantial contribution from (millennial) local-scale processes that do not include sediment compaction. If Swan Key had been the only site in South Florida where we reconstructed RSL, it is likely that we would have incorrectly interpreted this RSL trend as a regional signal, which demonstrates the potential pitfalls in the misattribution of trends to specific processes in the absence of within-region replication. Therefore, investigating within-core, within-site, and within-region replicability of RSL reconstructions is a constructive avenue for future research.

Supplementary data to this article can be found online at https://doi.org/10.1016/j.gloplacha.2022.103902.

## **Declaration of Competing Interest**

The authors declare that they have no known competing financial interests or personal relationships that could have appeared to influence the work reported in this paper.

#### Data availability

Data will be made available on request.

#### Acknowledgements

This work was supported by the Coastal and Marine Hazards and Resources Program and the Natural Hazards Mission Area, the Climate Research and Development Program of U.S. Geological Survey. Any use of trade, firm, or product names is for descriptive purposes only and does not imply endorsement by the U.S. Government. We thank Jaimie Shaw, Paulina Capar, and Anastasios Stathakapolous for assistance in the laboratory and field. Site access and research permission were provided by K. Watts for the Florida Keys National Wildlife Refuges Complex (Special Use Permit #FFO4RFKD-2015-020). Authors were supported by National Science Foundation Awards (OCE-1702587, OCE-1831450, and OCE-2002437 to Kopp and Ashe; OCE-2002431, OCE-1458921, OCE-1831382, and OCE-1942563 to Kemp; OCE-1458903 to Engelhart). RPM is supported by the US Fish and Wildlife Service's State Wildlife Grants Program (#F13AF00982). BPH is supported by the Singapore Ministry of Education Academic Research Fund MOE2019-T3-1-004 and MOE-T2EP50120-0007, the National Research Foundation Singapore, the Singapore Ministry of Education under the Research Centers of Excellence Initiative. Radiocarbon ages and descriptive core logs from SNK1 and SBC10 are available in a U.S. Geological Survey Data Release (https://doi.org/10.5066/P9OOL3L4). Data produced by non-USGS contributors are available upon request. This paper is a contribution to IGCP project 639 "Sea-level change from minutes to millennia," IGCP project 725 "Forecasting Coastal Change: From Cores to Code," PALSEA, and INQUA project 1601 "Geographic variability of Holocene relative sea level". This work comprises Earth Observatory of Singapore contribution no. 459.

### References

- Adams, P.N., Opdyke, N.D., Jaeger, J.M., 2010. Isostatic uplift driven by karstification and sea-level oscillation: modeling landscape evolution in North Florida. Geology 38. 531–534. https://doi.org/10.1130/G30592.1.
- Alexander, T.R., Crook, A.G., 1974. Recent vegetational changes in southern Florida. Environments of Southern Florida: present and past. Memoir 2, 61–72.
- Angulo, R.J., Giannini, P.C.F., Suguio, K., Pessenda, L.C.R., 1999. Relative sea-level changes in the last 5500 years in southern Brazil (Laguna–Imbituba region, Santa Catarina State) based on vermetid 14C ages. Mar. Geol. 159, 323–339. https://doi. org/10.1016/S0025-3227(98)00204-7
- Ashe, E.L., Cahill, N., Hay, C., Khan, N.S., Kemp, A., Engelhart, S.E., Horton, B.P., Parnell, A.C., Kopp, R.E., 2019. Statistical modeling of rates and trends in Holocene relative sea level. Quat. Sci. Rev. 204, 58–77. https://doi.org/10.1016/j. quascirev.2018.10.032.

- Barlow, N.L.M., Shennan, I., Long, A.J., Gehrels, W.R., Saher, M.H., Woodroffe, S.A., Hillier, C., 2013. Salt marshes as late Holocene tide gauges. Glob. Planet. Chang. 106, 90–110. https://doi.org/10.1016/j.gloplacha.2013.03.003.
- Barnett, R.L., Bernatchez, P., Garneau, M., Brain, M.J., Charman, D.J., Stephenson, D.B., Haley, S., Sanderson, N., 2019. Late Holocene sea-level changes in eastern Québec and potential drivers. Quat. Sci. Rev. 203, 151–169. https://doi.org/10.1016/j. guascirev.2018.10.039.
- Barnett, R.L., Bernatchez, P., Garneau, M., Juneau, M., 2017. Reconstructing late Holocene relative sea-level changes at the Magdalen Islands (Gulf of St. Lawrence, Canada) using multi-proxy analyses. J. Quat. Sci. 32 (3), 380–395. https://doi.org/ 10.1002/jns.2931
- Berkeley, A., Perry, C.T., Smithers, S.G., Horton, B.P., Cundy, A.B., 2009. Foraminiferal biofacies across mangrove-mudflat environments at Cocoa Creek, North Queensland, Australia. Mar. Geol. 263, 64–86. https://doi.org/10.1016/j.margeo.2009.03.019.
- Bloom, A.L., 1964. Peat accumulation and compaction in a Connecticut coastal marsh. J. Sediment. Res. 34.
- Bloom, A.L., 1970. Paludal stratigraphy of Truk, Ponape and Kusaie, Eastern Caroline Islands. Geol. Soc. Am. Bull. 81, 1895–1904.
- Boyer, J., Jones, R., 2001. The State of Florida bay Water Quality (1989–2001) (SERC Research Reports).
- Brain, M.J., 2015. Compaction, in: Handbook of Sea-Level Research. John Wiley & Sons, Ltd, pp. 452–469. https://doi.org/10.1002/9781118452547.ch30.
- Brain, M.J., Long, A.J., Petley, D.N., Horton, B.P., Allison, R.J., 2011. Compression behaviour of minerogenic low energy intertidal sediments. Sediment. Geol. 233, 28–41. https://doi.org/10.1016/j.sedgeo.2010.10.005.
- Brain, M.J., Kemp, A.C., Hawkes, A.D., Engelhart, S.E., Vane, C.H., Cahill, N., Hill, T.D., Donnelly, J.P., Horton, B.P., 2017. Exploring mechanisms of compaction in saltmarsh sediments using Common Era relative sea-level reconstructions. Quat. Sci. Rev. 167, 96–111. https://doi.org/10.1016/j.quascirev.2017.04.027.
- Bush, R., Dutton, A., Evans, M., Loft, R., Schmidt, G.A., 2020. Perspectives on data reproducibility and replicability in paleoclimate and climate science. Harvard Data Sci. Rev. 2 https://doi.org/10.1162/99608f92.00cd8f85.
- Cahoon, D.R., Hensel, P., Rybczyk, J., McKee, K.L., Proffitt, C.E., Perez, B.C., 2003. Mass tree mortality leads to mangrove peat collapse at Bay Islands, Honduras after Hurricane Mitch. J. Ecol. 91, 1093–1105. https://doi.org/10.1046/j.1365-2745.2003.00841.x.
- Carriquiry, J.D., Horta-Puga, G., 2010. The Ba/Ca record of corals from the Southern Gulf of Mexico: Contributions from land-use changes, fluvial discharge and oildrilling muds. Mar. Pollut. Bull. 60, 1625–1630. https://doi.org/10.1016/j.marpolbul.2010.06.007.
- Chamberlin, C.A., Bianchi, T.S., Brown, A.L., Cohen, M.J., Dong, X., Flint, M.K., Martin, J.B., McLaughlin, D.L., Murray, A.B., Pain, A., Quintero, C.J., Ward, N.D., Zhang, X., Heffernan, J.B., 2018. Mass balance implies Holocene development of a low-relief karst patterned landscape. Chem. Geol. https://doi.org/10.1016/j.chemgeo.2018.05.029.
- Christie, M.A., Bernhardt, C.E., Parnell, A.C., Shaw, T.A., Khan, N.S., Corbett, D.R., García-Artola, A., Clear, J., Walker, J.S., Donnelly, J.P., Hasse, T.R., Horton, B.P., 2021. Pollen geochronology from the Atlantic Coast of the United States during the last 500 years. Water 13, 362. https://doi.org/10.3390/w13030362.
- Chua, S., Switzer, A.D., Li, T., Chen, H., Christie, M., Shaw, T.A., Khan, N.S., Bird, M.I., Horton, B.P., 2021. A new Holocene sea-level record for Singapore. The Holocene. https://doi.org/10.1177/09596836211019096, 09596836211019096.
- Clark, J.A., Farrell, W.E., Peltier, W.R., 1978. Global changes in postglacial sea level: a numerical calculation. Quat. Res. 9, 265–287. https://doi.org/10.1016/0033-5894
- Coniglio, M., Harrison, R.S., 1983. Holocene and Pleistocene caliche from Big Pine Key, Florida. Bull. Can. Petrol. Geol. 31, 3–13.
- Conover, W.J., 1980. Practical Nonparametric Statistics. John Wiley & Sons.

  Creveling, J.R., Austermann, J., Dutton, A., 2019. Uplift of Trail Ridge, Florida, by karst dissolution, glacial isostatic adjustment, and dynamic topography. J. Geophys. Res. Solid Earth 124, 13354–13366. https://doi.org/10.1029/2019JB018489.
- Davis, R., Fitzgerald, D., 2003. Beaches and Coasts. Wiley.
- Dean, S., Horton, B.P., Evelpidou, N., Cahill, N., Spada, G., Sivan, D., 2019. Can we detect centennial sea-level variations over the last three thousand years in Israeli archaeological records? Quat. Sci. Rev. 210, 125–135. https://doi.org/10.1016/j. quascirev.2019.02.021.
- Debenay, J.-P., Guiral, D., Parra, M., 2004. Behaviour and taphonomic loss in foraminiferal assemblages of mangrove swamps of French Guiana. Mar. Geol. 208, 295–314. https://doi.org/10.1016/j.margeo.2004.04.013.
- Dekker, S.C., Boer, H.J., Dermody, B.J., Wagner-Cremer, F., Wassen, M.J., Eppinga, M.B., 2015. Holocene peatland initiation in the Greater Everglades. J. Geophys. Res. Biogeosci. 120, 254–269. https://doi.org/10.1002/2014JG002806.
- Desmond, G.B., 2003. Measuring and mapping the topography of the Florida Everglades for ecosystem restoration (USGS Numbered Series No. 021–03), Measuring and mapping the topography of the Florida Everglades for ecosystem restoration, Fact Sheet. Geol. Surv. (U.S.). https://doi.org/10.3133/fs02103.
- Dixon, T.H., Amelung, F., Ferretti, A., Novali, F., Rocca, F., Dokka, R., Sella, G., Kim, S.-W., Wdowinski, S., Whitman, D., 2006. Subsidence and flooding in New Orleans. Nature 441, 587–588. https://doi.org/10.1038/441587a.
- Dong, X., Cohen, M.J., Martin, J.B., McLaughlin, D.L., Murray, A.B., Ward, N.D., Flint, M. K., Heffernan, J.B., 2018. Ecohydrologic processes and soil thickness feedbacks control limestone-weathering rates in a karst landscape. Chem. Geol. https://doi.org/10.1016/j.chemgeo.2018.05.021.
- Ellison, J.C., 1993. Mangrove retreat with rising sea level, Bermuda. Estuar. Coast. Shelf Sci. 37, 75–87. https://doi.org/10.1006/ecss.1993.1042.

- Ellison, J.C., 2008. Long-term retrospection on mangrove development using sediment cores and pollen analysis: a review. Aquat. Bot. 89, 93–104. https://doi.org/ 10.1016/j.aquabot.2008.02.007.
- Ellison, J., Strickland, P., 2015. Establishing relative sea level trends where a coast lacks a long term tide gauge. Mitig. Adapt. Strateg. Glob. Chang. 20, 1211–1227.
- Faegri, K., Iversen, J., 1989. Textbook of Pollen Analysis. John Wiley & Sons Ltd.
- Froelich, P.N., Kaul, L.W., Byrd, J.T., Andreae, M.O., Roe, K.K., 1985. Arsenic, barium, germanium, tin, dimethylsulfide and nutrient biogeochemistry in Charlotte Harbor, Florida, a phosphorus-enriched estuary. Estuar. Coast. Shelf Sci. 20, 239–264. https://doi.org/10.1016/0272-7714(85)90041-1.
- Garrett, E., Melnick, D., Dura, T., Cisternas, M., Ely, L.L., Wesson, R.L., Jara-Muñoz, J., Whitehouse, P.L., 2020. Holocene relative sea-level change along the tectonically active Chilean coast. Quat. Sci. Rev. 236, 106281 https://doi.org/10.1016/j. quascirev.2020.106281.
- Gehrels, W.R., Hayward, B.W., Newnham, R.M., Southall, K.E., 2008. A 20th century acceleration of sea-level rise in New Zealand. Geophys. Res. Lett. 35 https://doi.org/ 10.1029/2007GL032632.
- Gehrels, W.R., Dangendorf, S., Barlow, N.L.M., Saher, M.H., Long, A.J., Woodworth, P.L., Piecuch, C.G., Berk, K., 2020. A preindustrial sea-level rise hotspot along the Atlantic Coast of North America. Geophys. Res. Lett. 47, e2019GL085814 https://doi.org/ 10.1029/2019GL085814.
- Gerlach, M.J., Engelhart, S.E., Kemp, A.C., Moyer, R.P., Smoak, J.M., Bernhardt, C.E., Cahill, N., 2017. Reconstructing common era relative sea-level change on the Gulf Coast of Florida. Mar. Geol. 390, 254–269. https://doi.org/10.1016/j. margeo.2017.07.001.
- Goodwin, I.D., Harvey, N., 2008. Subtropical sea-level history from coral microatolls in the Southern Cook Islands, since 300 AD. Mar. Geol. 253, 14–25. https://doi.org/ 10.1016/j.margeo.2008.04.012.
- Hall, G.F., Hill, D.F., Horton, B.P., Engelhart, S.E., Peltier, W.R., 2013. A high-resolution study of tides in the Delaware Bay: past conditions and future scenarios. Geophys. Res. Lett. 40, 338–342. https://doi.org/10.1029/2012GL054675.
- Hallmann, N., Camoin, G., Eisenhauer, A., Botella, A., Milne, G.A., Vella, C., Samankassou, E., Pothin, V., Dussouillez, P., Fleury, J., Fietzke, J., 2018. Ice volume and climate changes from a 6000 year sea-level record in French Polynesia. Nat. Commun. 9, 1–12. https://doi.org/10.1038/s41467-017-02695-7.
- Harris, P. Mitch, Purkis, S., Reyes, B., 2018. Statistical pattern analysis of surficial karst in the Pleistocene Miami oolite of South Florida. Sediment. Geol. 367, 84–95. https://doi.org/10.1016/j.sedgeo.2018.02.002.
- Haslett, J., Parnell, A., 2008. A simple monotone process with application to radiocarbon-dated depth chronologies. Journal of the Royal Statistical Society: Series C (Applied Statistics) 57, 399–418. https://doi.org/10.1111/j.1467-9876.2008.00623.x.
- Hawkes, A.D., Kemp, A.C., Donnelly, J.P., Horton, B.P., Peltier, W.R., Cahill, N., Hill, D. F., Ashe, E., Alexander, C.R., 2016. Relative sea-level change in northeastern Florida (USA) during the last ~8.0 ka. Quat. Sci. Rev. 142, 90–101. https://doi.org/10.1016/j.guascijev.2016.04.016.
- Head, K.H., 1988. Manual of Soil Laboratory Testing, Permeability, Shear Strength and Compressibility Tests, Vol. 2. Wiley, London.
- Head, K.H., Epps, R.J., 2011. Manual of Soil Laboratory Testing. Volume 2, Permeability, Shear Strength and Compressibility Tests, 3rd ed. Caithness, UK.
- Heaton, T.J., Köhler, P., Butzin, M., Bard, E., Reimer, R.W., Austin, W.E.N., Ramsey, C.B., Grootes, P.M., Hughen, K.A., Kromer, B., Reimer, P.J., Adkins, J., Burke, A., Cook, M. S., Olsen, J., Skinner, L.C., 2020. Marine20—the Marine radiocarbon age calibration curve (0–55,000 cal BP). Radiocarbon 62, 779–820. https://doi.org/10.1017/ RDC 2020 68
- Hickey, T.D., Hine, A.C., Shinn, E.A., Kruse, S.E., Poore, R.Z., 2010. Pleistocene carbonate stratigraphy of South Florida: evidence for High-Frequency Sea-Level Cyclicity. J. Coast. Res. 264, 605–614. https://doi.org/10.2112/JCOASTRES-D-09-005-21
- Hill, D.F., Griffiths, S.D., Peltier, W.R., Horton, B.P., Törnqvist, T.E., 2011. High-resolution numerical modeling of tides in the western Atlantic, Gulf of Mexico, and Caribbean Sea during the Holocene. J. Geophys. Res. 116 https://doi.org/10.1029/2010jc006896.
- Hobbs, N.B., 1986. Mire morphology and the properties and behaviour of some British and foreign peats. Quart. J. Eng. Geol. 19, 7–80. https://doi.org/10.1144/GSL. OJEG.1986.019.01.02.
- Hoffman, M.L., Collopy, M.W., 1988. Historical status of the American Kestrel (Falco sparverius paulus) in Florida. Wilson Bull. 100, 91–107.
- Horton, B.P., Edwards, R.J., 2005. The application of local and regional transfer functions to the reconstruction of Holocene sea levels, North Norfolk, England. Holocene 15, 216–228. https://doi.org/10.1191/0959683605hl787rp.
- Horton, B.P., Edwards, R.J., 2006. Quantifying Holocene sea-level change using intertidal foraminifera. In: Lessons from the British Isles. Cushman Foundation for Foraminiferal Research.
- Horton, B.P., Larcombe, P., Woodroffe, S.A., Whittaker, J.E., Wright, M.R., Wynn, C., 2003. Contemporary foraminiferal distributions of a mangrove environment, Great Barrier Reef coastline, Australia: implications for sea-level reconstructions. Mar. Geol. 198, 225–243. https://doi.org/10.1016/S0025-3227(03)00117-8.
- Horton, B.P., Whittaker, J.E., Thomson, K.H., Hardbattle, M.I.J., Kemp, A., Woodroffe, S. A., Wright, M.R., 2005. The development of a modern foraminiferal data set for sealevel reconstructions, Wakatobi Marine National Park, Southeast Sulawesi, Indonesia. J. Foraminifer. Res. 35, 1–14. https://doi.org/10.2113/35.1.1.
- Huck, R.B., 1995. A centennial review: the historic natural landscape of Key Biscayne, Dade County, Florida. Florida Sci. 58, 335–351.
- Johannes, J.H., 1976. Yesterday's Reflections: Nassau County, Florida: A Pictorial History (TO Richardson).

- Johnson, C.S., Miller, K.G., Browning, J.V., Kopp, R.E., Khan, N.S., Fan, Y., Stanford, S. D., Horton, B.P., 2018. The role of sediment compaction and groundwater withdrawal in local sea-level rise, Sandy Hook, New Jersey, USA. Quat. Sci. Rev. 181, 30–42. https://doi.org/10.1016/j.quascirev.2017.11.031.
- Jones, M.C., Wingard, G.L., Stackhouse, B., Keller, K., Willard, D., Marot, M., Landacre, B., Bernhardt, E.C., 2019. Rapid inundation of southern Florida coastline despite low relative sea-level rise rates during the late-Holocene. Nat. Commun. 10, 3231. https://doi.org/10.1038/s41467-019-11138-4.
- Karegar, M.A., Dixon, T.H., Engelhart, S.E., 2016. Subsidence along the Atlantic Coast of North America: Insights from GPS and late Holocene relative sea level data. Geophys. Res. Lett. 43, 3126–3133. https://doi.org/10.1002/2016GL068015.
- Kaye, C.A., Barghoorn, E.S., 1964. Late Quaternary sea-level change and crustal rise at Boston, Massachusetts, with notes on the autocompaction of peat. Bull. Geol. Soc. Am. 75, 63–80. https://doi.org/10.1130/0016-7606(1964)75[63:LQSCAC]2.0.CO;
- Kelsey, H.M., 2015. Geomorphological indicators of past sea levels. In: Shennan, I., Long, A.J., Horton, B.P. (Eds.), Handbook of Sea-Level Research. John Wiley & Sons, Ltd, pp. 66–82.
- Kemp, A.C., Nelson, A.R., Horton, B.P., 2013b. 14.31 Radiocarbon dating of plant macrofossils from tidal-marsh sediment. In: Shroder, J.F. (Ed.), Treatise on Geomorphology. Academic Press, San Diego, pp. 370–388.
- Kemp, A.C., Shaw, T.A., Piecuch, C.G., 2022. The importance of non-tidal water-level variability for reconstructing Holocene relative sea level. Quat. Sci. Rev. 290, 107637. https://doi.org/10.1016/j.quascirev.2022.107637.
- Kemp, A.C., Telford, R.J., 2015. Transfer Functions, in: Handbook of Sea-Level Research. John Wiley & Sons, Ltd, pp. 470–499. https://doi.org/10.1002/9781118452547. ch31.
- Kemp, A.C., Hawkes, A.D., Vane, C.H., Horton, B.P., Hill, T.D., Anisfeld, S.C., Parnell, A. C., Cahill, N., 2015. Relative sea-level change in Connecticut (USA) during the last 2200 yrs. Earth and Planet. Sci. Lett. 428, 217–229. https://doi.org/10.1016/j.epsl.2015.07.034.
- Kemp, A.C., Hill, T.D., Vane, C.H., Cahill, N., Orton, P.M., Talke, S.A., Parnell, A.C., Sanborn, K., Hartig, E.K., 2017a. Relative sea-level trends in New York City during the past 1500 years. The Holocene 27 (8), 1169–1186. https://doi.org/10.1177/ 0959683616683263.
- Kemp, A.C., Horton, B.P., Donnelly, J.P., Mann, M.E., Vermeer, M., Rahmstorf, S., 2011. Climate related sea-level variations over the past two millennia. PNAS 108, 11017–11022. https://doi.org/10.1073/pnas.1015619108.
- Kemp, A.C., Kegel, J.J., Culver, S.J., Barber, D.C., Mallinson, D.J., Leorri, E., Bernhardt, C.E., Cahill, N., Riggs, S.R., Woodson, A.L., Mulligan, R.P., Horton, B.P., 2017b. Extended late Holocene relative sea-level histories for North Carolina, USA. Quat. Sci. Rev. 160, 13–30. https://doi.org/10.1016/j.quascirev.2017.01.012.
- Kemp, A.C., Bernhardt, C.E., Horton, B.P., Kopp, R.E., Vane, C.H., Peltier, W.R., Hawkes, A.D., Donnelly, J.P., Parnell, A.C., Cahill, N., 2014. Late Holocene sea- and land-level change on the U.S. southeastern Atlantic coast. Mar. Geol. 357, 90–100. https://doi.org/10.1016/j.margeo.2014.07.010.
- Kemp, A.C., Wright, A.J., Edwards, R.J., Barnett, R.L., Brain, M.J., Kopp, R.E., Cahill, N., Horton, B.P., Charman, D.J., Hawkes, A.D., Hill, T.D., van de Plassche, O., 2018. Relative sea-level change in Newfoundland, Canada during the past ~3000 years. Ouat. Sci. Rev. 201, 89–110. https://doi.org/10.1016/j.quascirev.2018.10.012.
- Kemp, A.C., Vane, C.H., Khan, N.S., Ellison, J.C., Engelhart, S.E., Horton, B.P., Nikitina, D., Smith, S.R., Rodrigues, L.J., Moyer, R.P., 2019. Testing the utility of geochemical proxies to reconstruct Holocene coastal environments and relative sea level: a case study from Hungry Bay, Bermuda. Open Quatern. 5, 1. https://doi.org/ 10.5334/op.49
- Kemp, A.C., Wright, A.J., Cahill, N., 2020. Enough is enough, or more is more? Testing the influence of foraminiferal count size on reconstructions of paleo-marsh elevation. J. Foraminifer. Res. 50, 266–278. https://doi.org/10.2113/gsjfr.50.3.266.
- Khan, N.S., Ashe, E., Shaw, T.A., Vacchi, M., Walker, J., Peltier, W.R., Kopp, R.E., Horton, B.P., 2015. Holocene relative sea-level changes from near-, intermediate-, and far-field locations. Curr. Clim. Change Rep. 1, 247–262. https://doi.org/ 10.1007/s40641-015-0029-z.
- Kemp, A.C., Horton, B.P., Vane, C.H., Bernhardt, C.E., Corbett, D.R., Engelhart, S.E., Anisfeld, S.C., Parnell, A.C., Cahill, N., 2013a. Sea-level change during the last 2500 years in New Jersey, USA. Quat. Sci. Rev. 81, 90–104. https://doi.org/10.1016/j. quascirev.2013.09.024.
- Khan, N.S., Ashe, E., Horton, B.P., Dutton, A., Kopp, R.E., Brocard, G., Engelhart, S.E., Hill, D.F., Peltier, W.R., Vane, C.H., Scatena, F.N., 2017. Drivers of Holocene sealevel change in the Caribbean. Quat. Sci. Rev. 155, 13–36. https://doi.org/10.1016/ i.quascirev.2016.08.032.
- Khan, N.S., Vane, C.H., Engelhart, S.E., Kendrick, C., Horton, B.P., 2019. The application of  $\delta$ 13C, TOC and C/N geochemistry of mangrove sediments to reconstruct Holocene paleoenvironments and relative sea levels. Puerto Rico. Mar. Geol. 415, 105963 https://doi.org/10.1016/j.margeo.2019.105963.
- Khan, N.S., Toth, L.T., Moyer, R.P., Shaw, J.E., Capar, P., Kemp, A.C., Engelhart, S.E., Horton, B.P., 2022. Mangrove peat radiocarbon ages from Snipe and Swan Key, FL. U.S. Geological Survey data release. https://doi.org/10.5066/P9OOL3L4.
- Kolker, A.S., Allison, M.A., Hameed, S., 2011. An evaluation of subsidence rates and sealevel variability in the northern Gulf of Mexico. Geophys. Res. Lett. 38 https://doi.org/10.1029/2011GL049458.
- Kopp, R.E., Kemp, A.C., Bittermann, K., Horton, B.P., Donnelly, J.P., Gehrels, W.R., Hay, C.C., Mitrovica, J.X., Morrow, E.D., Rahmstorf, S., 2016. Temperature-driven global sea-level variability in the Common Era. PNAS 113, E1434–E1441. https:// doi.org/10.1073/pnas.1517056113.
- Kuchar, J., Milne, G., Wolstencroft, M., Love, R., Tarasov, L., Hijma, M., 2018. The influence of sediment isostatic adjustment on sea level change and land motion along

- the U.S. Gulf Coast. J. Geophys. Res. Solid Earth 123, 780–796. https://doi.org/ 10.1002/2017JB014695.
- Lamoreaux, P.E., Newton, J.G., 1986. Catastrophic subsidence: an environmental hazard, shelby county, Alabama. Environ. Geol. Water Sci. 8, 25–40. https://doi.org/ 10.1007/BE02525556
- Lauredo, M., 2018. Dade County Slash Pine. Coral Gables Museum. URL. https://coralgablesmuseum.org/portfolio-item/dade-county-slash-pine/ (accessed 7.24.22).
- Leong, R.C., Friess, D.A., Crase, B., Lee, W.K., Webb, E.L., 2018. High-resolution pattern of mangrove species distribution is controlled by surface elevation. Estuar. Coast. Shelf Sci. 202, 185–192. https://doi.org/10.1016/j.ecss.2017.12.015.
- Liu, Y., Weisberg, R.H., 2012. Seasonal variability on the West Florida Shelf. Prog. Oceanogr. 104, 80–98. https://doi.org/10.1016/j.pocean.2012.06.001.
- Long, A.J., Woodroffe, S.A., Milne, G.A., Bryant, C.L., Simpson, M.J.R., Wake, L.M., 2012. Relative Sea-level change in Greenland during the last 700yrs and ice sheet response to the Little Ice Age. In: Earth and Planetary Science Letters, Sea Level and Ice Sheet Evolution: A PALSEA Special Edition, 315–316, pp. 76–85. https://doi.org/ 10.1016/j.epsl.2011.06.027.
- Love, R., Milne, G.A., Tarasov, L., Engelhart, S.E., Hijma, M.P., Latychev, K., Horton, B. P., Törnqvist, T.E., 2016. The contribution of glacial isostatic adjustment to projections of sea-level change along the Atlantic and Gulf coasts of North America. Earth's Future 4, 440–464. https://doi.org/10.1002/2016EF000363.
- Lugo, A.E., Snedaker, S.C., 1974. The Ecology of Mangroves. Annu. Rev. Ecol. Syst. 5, 39–64. https://doi.org/10.1146/annurev.es.05.110174.000351.
- Madden, M., Jones, D., Vilchek, L., 1999. Photointerpretation key for the everglades vegetation classification system. Photogramm. Eng. Remote. Sens. 65, 171–177.
- Marshall, F.E., Bernhardt, C.E., Wingard, G.L., 2020. Estimating late 19th century hydrology in the greater everglades ecosystem: an integration of paleoecologic data and models. Front. Environ. Sci. 8.
- Maul, G.A., Martin, D.M., 1993. Sea level rise at Key West, Florida, 1846-1992: America's longest instrument record? Geophys. Res. Lett. 20, 1955–1958. https://doi.org/10.1029/93GL02371.
- McAllister, B., 1938. A Study of the Flora of Key Biscayne, Dade County, Florida. M.A. Thesis. Duke University, Durham, N.C.
- McHutchon, A., Rasmussen, C.E., 2011. Gaussian Process Training with Input Noise. In: Shawe-Taylor, J., Zemel, R.S., Bartlett, P.L., Pereira, F., Weinberger, K.Q. (Eds.), Advances in Neural Information Processing Systems 24. Curran Associates, Inc., pp. 1341–1349
- McKee, K.L., Cahoon, D.R., Feller, I.C., 2007. Caribbean mangroves adjust to rising sea level through biotic controls on change in soil elevation. Global Ecol. Biogeograph. 16, 545–556. https://doi.org/10.1111/j.1466-8238.2007.00317.x.
- McKee, K.L., Faulkner, P.L., 2000. Mangrove Peat Analysis and Reconstruction of Vegetation History at the Pelican Cays. Belize.
- McPherson, B.F., Halley, R.B., 1996. The South Florida environment: A region under stress (USGS Numbered Series no. 1134). In: The South Florida Environment: A Region under Stress, Circular. U.S. Geological Survey, Reston, VA. https://doi.org/ 10.3133/cir.1134.
- Miller, J.A., 1990. Ground Water Atlas of the United States: Segment 6, Alabama, Florida, Georgia, South Carolina (USGS Numbered Series no. 730-G). In: Ground Water Atlas of the United States: Segment 6. Hydrologic Atlas. U.S. Geological Survey, Alabama, Florida, Georgia, South Carolina. https://doi.org/10.3133/ ha730G.
- Milne, G.A., Long, A.J., Bassett, S.E., 2005. Modelling Holocene relative sea-level observations from the Caribbean and South America. Quat. Sci. Rev. 24, 1183–1202. https://doi.org/10.1016/j.quascirev.2004.10.005.
- Morton, J.F., 1980. The Australian pine or beefwood (Casuarina equisetifolia L.) an invasive "weed" tree in Florida. In: Proceedings of the Florida State Horticultural Society, pp. 87–95.
- Niering, W., Warren, R., Weymouth, C., 1977. Our dynamic tidal marshes: vegetation changes as revealed by peat analysis. In: The Connecticult Arboretum Bulletin Bulletin No. 22.
- Noss, R.F., 2011. Between the devil and the deep blue sea: Florida's unenviable position with respect to sea level rise. Clim. Chang. 107, 1–16. https://doi.org/10.1007/s10584-011-0109-6
- Odum, W.E., McIvor, C.C., Iii, T.J.S., 1982. The Ecology of the Mangroves of South Florida: A Community Profile (No. 81/24), FWS/OBS. U.S. Fish and Wildlife Service.
- Ono, K., Hiradate, S., Morita, S., Hiraide, M., Hirata, Y., Fujimoto, K., Tabuchi, R., Lihpai, S., 2015. Assessing the carbon compositions and sources of mangrove peat in a tropical mangrove forest on Pohnpei Island, Federated States of Micronesia. GEODERMA 245–246, 11–20. https://doi.org/10.1016/j.geoderma.2015.01.008.
- Opdyke, N.D., Spangler, D.P., Smith, D.L., Jones, D.S., Lindquist, R.C., 1984. Origin of the epeirogenic uplift of Pliocene-Pleistocene beach ridges in Florida and development of the Florida karst. Geology 12, 226–228. https://doi.org/10.1130/0091-7613(1984)12<226:OOTEUO>2.0.CO;2.
- Parnell, A.C., Buck, C.E., Doan, T.K., 2011. A review of statistical chronology models for high-resolution, proxy-based Holocene palaeoenvironmental reconstruction. Quat. Sci. Rev. 30, 2948–2960.
- Peltier, W.R., 1996. Global sea level rise and glacial isostatic adjustment: an analysis of data from the East Coast of North America. Geophys. Res. Lett. 23, 717–720. https:// doi.org/10.1029/96GL00848.
- Peltier, W.R., 2004. Global glacial isostasy and the surface of the ICE-age earth: the ICE-5G (VM2) model and GRACE. Annu. Rev. Earth Planet. Sci. 32, 111.
- Peltier, W.R., Argus, D.F., Drummond, R., 2015. Space geodesy constrains ice age terminal deglaciation: The global ICE-6G\_C (VM5a) model. J. Geophys. Res. Solid Earth 120, 450–487. https://doi.org/10.1002/2014JB011176.

- Piecuch, C.G., Huybers, P., Hay, C.C., Kemp, A.C., Little, C.M., Mitrovica, J.X., Ponte, R. M., Tingley, M.P., 2018. Origin of spatial variation in US East Coast sea-level trends during 1900–2017. Nature 564, 400. https://doi.org/10.1038/s41586-018-0787-6.
- Plater, A.J., Kirby, J.R., Boyle, J.F., Shaw, T., Mills, H., 2015. Loss on ignition and organic content. In: Handbook of Sea-Level Research. John Wiley & Sons, Ltd, pp. 312–330. https://doi.org/10.1002/9781118452547.ch21.
- Punwong, P., Marchant, R., Selby, K., 2013. Holocene mangrove dynamics in Makoba Bay, Zanzibar. Palaeogeogr. Palaeoclimatol. Palaeoecol. 379–380, 54–67. https:// doi.org/10.1016/j.palaeo.2013.04.004.
- Coastal habitat integrated mapping and monitoring program report for the state of Florida. In: Radabaugh, K.R., Powell, C.E., Moyer, R.P. (Eds.), 2017. Florida Fish and Wildlife Conservation Commission Technical Report No. 21. Fish and Wildlife Research Institute. https://myfwc.com/research/habitat/coastal-wetlands/chimmp/.
- Ramcharan, E.K., McAndrews, J.H., 2006. Holocene Development of Coastal Wetland at Maracas Bay, Trinidad, West Indies. J. Coastal Res. 581–586. https://doi.org/ 10.2112/04A-0001.1.
- Rasmussen, C., Williams, C., 2006. Gaussian Processes for Machine Learning. MIT Press, Cambridge, MA.
- Rees, S., 2014. Adaptive oedometer automation. Geotechnica 27-32.
- Reimer, P.J., Austin, W.E.N., Bard, E., Bayliss, A., Blackwell, P.G., Ramsey, C.B., Butzin, M., Cheng, H., Edwards, R.L., Friedrich, M., Grootes, P.M., Guilderson, T.P., Hajdas, I., Heaton, T.J., Hogg, A.G., Hughen, K.A., Kromer, B., Manning, S.W., Muscheler, R., Palmer, J.G., Pearson, C., van der Plicht, J., Reimer, R.W., Richards, D.A., Scott, E.M., Southon, J.R., Turney, C.S.M., Wacker, L., Adolphi, F., Büntgen, U., Capano, M., Fahrni, S.M., Fogtmann-Schulz, A., Friedrich, R., Köhler, P., Kudsk, S., Miyake, F., Olsen, J., Reinig, F., Sakamoto, M., Sookdeo, A., Talamo, S., 2020. The IntCal20 Northern Hemisphere radiocarbon age calibration curve (0–55 cal kBP). Radiocarbon 62, 725–757. https://doi.org/10.1017/RDC.2020.41.
- Rivera-Monroy, V.H., Danielson, T.M., Castañeda-Moya, E., Marx, B.D., Travieso, R., Zhao, X., Gaiser, E.E., Farfan, L.M., 2019. Long-term demography and stem productivity of Everglades mangrove forests (Florida, USA): resistance to hurricane disturbance. For. Ecol. Manag. 440, 79–91. https://doi.org/10.1016/j. foreco.2019.02.036.
- Robbin, D.M., 1984. A New Holocene Sea level curve for Upper Florida Keys and Florida Reef Tract. AAPG Bull. 68 https://doi.org/10.1306/AD46113D-16F7-11D7-8645000102C1865D.
- Rovai, A.S., Twilley, R.R., Castañeda-Moya, E., Riul, P., Cifuentes-Jara, M., Manrow-Villalobos, M., Horta, P.A., Simonassi, J.C., Fonseca, A.L., Pagliosa, P.R., 2018. Global controls on carbon storage in mangrove soils. Nat. Clim. Chang. 8, 534–538. https://doi.org/10.1038/s41558-018-0162-5.
- Roy, K., Peltier, W.R., 2017. Space-geodetic and water level gauge constraints on continental uplift and tilting over North America: regional convergence of the ICE-6G\_C (VM5a/VM6) models. Geophys. J. Int. 210, 1115–1142. https://doi.org/ 10.1093/gii/ggx156.
- Runge, E.C.A., Goli, K.M., Rafter, T.A., 1973. Radiocarbon chronology and problems in its interpretation for quaternary loess deposits-South Canterbury, New Zealand. Soil Sci. Soc. Am. J. 37, 742–746. https://doi.org/10.2136/ sssail973.03615995003700050032x
- Saintilan, N., Wilson, N.C., Rogers, K., Rajkaran, A., Krauss, K.W., 2014. Mangrove expansion and salt marsh decline at mangrove poleward limits. Glob. Chang. Biol. 20, 147–157. https://doi.org/10.1111/gcb.12341.
- Saintilan, N., Khan, N.S., Ashe, E., Kelleway, J.J., Rogers, K., Woodroffe, C.D., Horton, B. P., 2020. Thresholds of mangrove survival under rapid sea level rise. Science 368, 1118–1121. https://doi.org/10.1126/science.aba2656.
- Sanford, S., 1909. The Topography and Geology of Southern Florida, Florida Geological Survey Annual Report.
- Scholl, D.W., 1964. Recent sedimentary record in mangrove swamps and rise in sea level over the southwestern coast of Florida: part 2. Mar. Geol. 2, 343–364. https://doi. org/10.1016/0025-3227(64)90047-7.
- Scott, T.M., 2001. Text to Accompany the Geologic Map of Florida (Open File Report No. 99). Florida Geological Survey.
- Sefton, J., Woodroffe, S., Ascough, P., Khan, N., 2022. Reliability of mangrove radiocarbon chronologies: a case study from Mahé. Seychelles. Holoc. 32 (6), 529–542
- Shore, J.S., Bartley, D.D., Harkness, D.D., 1995. Problems encountered with the 14C dating of peat. Quat. Sci. Rev. 14, 373–383. https://doi.org/10.1016/0277-3791 (95)00031-3.
- Sivan, D., Lambeck, K., Toueg, R., Raban, A., Porath, Y., Shirman, B., 2004. Ancient coastal wells of Caesarea Maritima, Israel, an indicator for relative sea level changes during the last 2000 years. Earth Planet. Sci. Lett. 222, 315–330. https://doi.org/10.1016/j.epsl.2004.02.007.
- Smith, N.P., 1994. Long-term Gulf-to-Atlantic transport through tidal channels in the Florida Keys. Bull. Mar. Sci. 54, 602–609.
- Spalding, M., Kainuma, M., Collins, L., 2010. World Atlas of Mangroves (Earthscan).
- Stathakopoulos, A., Riegl, B.M., Toth, L.T., 2020. A revised Holocene coral sea-level database from the Florida reef tract, USA. PeerJ 8, e8350. https://doi.org/10.7717/ peerj.8350.
- Suguio, K., Martin, L., 1978. Formações quaternária marinhas do litoral paulista e sul fluminense. In: Int. Symp. on Coastal Evolution in the Quaternary, São Paulo. Spec. Publ., no. 1. São Paulo, IGCP, Project 61, 55. Instituto de Geociências, Universidade de São Paulo.
- Swart, P.K., Healy, G., Greer, L., Lutz, M., Saied, A., Anderegg, D., Dodge, R.E., Rudnick, D., 1999. The use of proxy chemical records in coral skeletons to ascertain

- past environmental conditions in Florida Bay. Estuaries 22, 384–397. https://doi.org/10.2307/1353206.
- Swarzenski, P.W., Baskaran, M., Rosenbauer, R.J., Orem, W.H., 2006a. Historical trace element distribution in sediments from the Mississippi River delta. Estuar. Coasts: J ERF 29, 1094–1107. https://doi.org/10.1007/BF02781812.
- Swarzenski, P.W., Orem, W.H., McPherson, B.F., Baskaran, M., Wan, Y., 2006b. Biogeochemical transport in the Loxahatchee River estuary, Florida: the role of submarine groundwater discharge. Mar. Chem. 101, 248–265. https://doi.org/ 10.1016/j.marchem.2006.03.007.
- Thom, B.G., 1967. Mangrove ecology and deltaic geomorphology: Tabasco, Mexico. J. Ecol. 55, 301–343. https://doi.org/10.2307/2257879.
- Tomlinson, P.B., 2016. The Botany of Mangroves. Cambridge University Press.
- Toscano, M.A., Gonzalez, J.L., Whelan, K.R.T., 2018. Calibrated density profiles of Caribbean mangrove peat sequences from computed tomography for assessment of peat preservation, compaction, and impacts on sea-level reconstructions. Quat. Res. 89, 201–222. https://doi.org/10.1017/qua.2017.101.
- Toscano, M.A., Macintyre, I.G., 2003. Corrected western Atlantic sea-level curve for the last 11,000 years based on calibrated C-14 dates from Acropora palmata framework and intertidal mangrove peat. Coral Reefs 22, 257–270. https://doi.org/10.1007/ S00338.003.0315.4
- Toth, L.T., Cheng, H., Edwards, R.L., Ashe, E., Richey, J.N., 2017a. Local Radiocarbon Reservoir Age (Delta-R) Variability from the Nearshore and Open-Ocean Environments of the Florida Keys Reef Tract during the Holocene and Associated U-Series and Radiocarbon Data. https://doi.org/10.5066/F7P8492Q.
- Toth, L.T., Cheng, H., Edwards, R.L., Ashe, E., Richey, J.N., 2017b. Millennial-scale variability in the local radiocarbon reservoir age of South Florida during the Holocene. Quat. Geochronol. 42, 130–143. https://doi.org/10.1016/j.guageo.2017.07.005.
- van de Plassche, O., van der Borg, K., de Jong, A.F.M., 1998. Sea level-climate correlation during the past 1400 yr. Geology 26, 319–322. https://doi.org/10.1130/0091-7613(1998)026<0319;SLCCDT>2.3.CO;2.
- Volk, M., Hoctor, T., Nettles, B., Hilsenbeck, R., Putz, F., 2017. Florida land use and land cover change in the past 100 years. In: Florida's Climate: Changes, Variations, & Impacts. Florida Climate Institute. https://doi.org/10.17125/fci2017.ch02.
- Walker, J.S., Kopp, R.E., Shaw, T.A., Cahill, N., Khan, N.S., Barber, D.C., Ashe, E.L., Brain, M.J., Clear, J.L., Corbett, D.R., Horton, B.P., 2021. Common Era Sea-level budgets along the U.S. Atlantic coast. Nat. Commun. 12, 1841. https://doi.org/ 10.1038/s41467-021-22079-2.
- Waltham, A.C., Fookes, P.G., 2003. Engineering classification of karst ground conditions. Q. J. Eng. Geol. Hydrogeol. 36, 101–118. https://doi.org/10.1144/1470-9236/ 2002.33
- Weerabaddana, M.M., DeLong, K.L., Wagner, A.J., Loke, D.W.Y., Kilbourne, K.H., Slowey, N., Hu, H.-M., Shen, C.-C., 2021. Insights from barium variability in a Siderastrea siderea coral in the northwestern Gulf of Mexico. Mar. Pollut. Bull. 173, 112930 https://doi.org/10.1016/j.marpolbul.2021.112930.
- Welch, R., Madden, M., Doren, R.F., 1999. Mapping the Everglades. PE&RS, Photogrammetric Engineering Remote Sensing, 65, pp. 163–170.
- Whitmore, T.J., Riedinger-Whitmore, M.A., Smoak, J.M., Kolasa, K.V., Goddard, E.A., Bindler, R., 2008. Arsenic contamination of lake sediments in Florida: evidence of herbicide mobility from watershed soils. J. Paleolimnol. 40, 869–884. https://doi. org/10.1007/s10933-008-9204-8.

- Wild, E., Steier, P., Fischer, P., Höflmayer, F., 2013. 14C dating of humic acids from bronze and iron age plant remains from the Eastern Mediterranean. Radiocarbon 55, 599–607. https://doi.org/10.1017/S003382220005774X.
- Willard, D.A., Bernhardt, C.E., 2011. Impacts of past climate and sea level change on Everglades wetlands: placing a century of anthropogenic change into a late-Holocene context. Clim. Chang. 107, 59–80. https://doi.org/10.1007/s10584-011-0078-9.
- Wingard, G.L., Hudley, J.W., Holmes, C.W., Willard, D.A., Marot, M., 2007. Synthesis of age data and chronology for Florida Bay and Biscayne Bay Cores collected for the Ecosystem history of South Florida's Estuaries Projects. In: US Geological Survey, Open File Report, 1203, pp. 1203–2007.
- Wojeck, G.A., Nigg, H.N., Braman, R.S., Stamper, J.H., Rouseff, R.L., 1982. Worker exposure to arsenic in Florida grapefruit spray operations. Arch. Environ. Contam. Toxicol. 11, 661–667. https://doi.org/10.1007/BF01059152.
- Wolstencroft, M., Shen, Z., Törnqvist, T.E., Milne, G.A., Kulp, M., 2014. Understanding subsidence in the Mississippi Delta region due to sediment, ice, and ocean loading: Insights from geophysical modeling: modeling load-induced subsidence. J. Geophys. Res. Solid Earth 119, 3838–3856. https://doi.org/10.1002/2013JB010928.
- Woodroffe, C.D., 1981. Mangrove swamp stratigraphy and Holocene transgression, Grand Cayman Island, West Indies. Marine Geol 41, 271–294. https://doi.org/ 10.1016/0025-3227(81)90085-2.
- Woodroffe, C.D., McGregor, H.V., Lambeck, K., Smithers, S.G., Fink, D., 2012. Mid-Pacific microatolls record sea-level stability over the past 5000 yr. Geology 40, 951–954. https://doi.org/10.1130/G33344.1.
- Woodroffe, S.A., Long, A.J., Milne, G.A., Bryant, C.L., Thomas, A.L., 2015a. New constraints on late Holocene eustatic sea-level changes from Mahé, Seychelles. Quat. Sci. Rev. 115, 1–16. https://doi.org/10.1016/j.quascirev.2015.02.011.
- Woodroffe, S.A., Long, A.J., Punwong, P., Selby, K., Bryant, C.L., Marchant, R., 2015b. Radiocarbon dating of mangrove sediments to constrain Holocene relative sea-level change on Zanzibar in the Southwest Indian Ocean. The Holocene 25, 820–831. https://doi.org/10.1177/0959683615571422.
- Woodroffe, C.D., Rogers, K., McKee, K.L., Lovelock, C.E., Mendelssohn, I.A., Saintilan, N., 2016. Mangrove sedimentation and response to relative sea-level rise. Annu. Rev. Mar. Sci. 8, 243–266. https://doi.org/10.1146/annurev-marine-122414-034025.
- Yang, Z., Myers, I., Jeong, S., White, S., 2012. VDatum for coastal waters from the Florida Shelf to the South Atlantic Bight: Tidal datums, marine grids, and sea surface topography (NOAA Techinal Memorandum No. NOS CS 27).
- Yao, Q., Liu, K., Rodrigues, E., Bianchette, T., Aragón-Moreno, A.A., Zhang, Z., 2020. A geochemical record of Late-Holocene hurricane events from the Florida Everglades. Water Resour. Res. 56, e2019WR026857 https://doi.org/10.1029/ 2019WR026857
- Zhang, X., Bianchi, T.S., Cohen, M.J., Martin, J.B., Quintero, C.J., Brown, A.L., Ares, A. M., Heffernan, J.B., Ward, N., Osborne, T.Z., Shields, M.R., Kenney, W.F., 2019. Initiation and Development of Wetlands in Southern Florida Karst Landscape Associated With Accumulation of Organic Matter and Vegetation Evolution. J. Geophys. Res. Biogeosci. 124, 1604–1617. https://doi.org/10.1029/2018.IG004921.
- Zieman, Jr, Joseph, C., 1972. Origin of circular beds of Thalassia (Spermatophyta: Hydrocharitaceae) in South Biscayne Bay, Florida, and their Relationship to Mangrove Hammocks. Bull. Mar. Sci. 22, 559–574.